

1 Large-scale sensitivities of groundwater and surface water to 2 groundwater withdrawal

3
4 *Marc F.P. Bierkens^{1,2,#}, Edwin H. Sutanudjaja¹ and Niko Wanders¹*

5
6 ¹Department of Physical Geography, Utrecht University, P.O. Box 80115, 3508 TC Utrecht,
7 The Netherlands

8 ²Unit Soil and Groundwater Systems, Deltares, P.O. Box 85467, 3508 AL Utrecht, The
9 Netherlands

10 # Correspondence to: m.f.p.bierkens@uu.nl

13 **Abstract**

14 Increasing population, economic growth and changes in diet have dramatically increased the
15 demand for food and water over the last decades. To meet increasing demands, irrigated
16 agriculture has expanded into semi-arid areas with limited precipitation and surface water
17 availability. This has greatly intensified the dependence of irrigated crops on groundwater
18 withdrawal and caused a steady increase of groundwater withdrawal and groundwater
19 depletion. One of the effects of groundwater pumping is the reduction in streamflow through
20 capture of groundwater recharge, with detrimental effects on aquatic ecosystems. The degree
21 to which groundwater withdrawal affects streamflow or groundwater storage depends on the
22 nature of the groundwater-surface water interaction (GWSI). So far, analytical solutions that
23 have been derived to calculate the impact of groundwater on streamflow depletion involve
24 single wells and streams and do not allow the GWSI to shift from connected to disconnected,
25 i.e. from a situation with two-way interaction to one with a one-way interaction between
26 groundwater and surface water. Including this shift and also analyse the effects of many
27 wells, requires numerical groundwater models that are expensive to setup. Here, we introduce
28 an analytical framework based on a simple lumped conceptual model that allows to estimate
29 to what extent groundwater withdrawal affects groundwater heads and streamflow at regional
30 scales. It accounts for a shift in GWSI, calculates at which critical withdrawal rate such a
31 shift is expected and when it is likely to occur after withdrawal commences. It also provides
32 estimates of streamflow depletion and which part of the groundwater withdrawal comes out
33 of groundwater storage and which parts from a reduction in streamflow. After a local
34 sensitivity analysis, the framework is combined with parameters and inputs from a global
35 hydrological model and subsequently used to provide global maps of critical withdrawal rates
36 and timing, the areas where current withdrawal exceeds critical limits, and maps of
37 groundwater depletion and streamflow depletion rates that result from groundwater

38 withdrawal. The resulting global depletion rates are compared with estimates from in situ-
39 observations, regional and global groundwater models and satellites. Pairing of the analytical
40 framework with more complex global hydrological models presents a screening tool for fast
41 first-order assessments of regional-scale groundwater sustainability, and for supporting
42 hydroeconomic models that require simple relationships between groundwater withdrawal
43 rates and the evolution of pumping costs and environmental externalities.

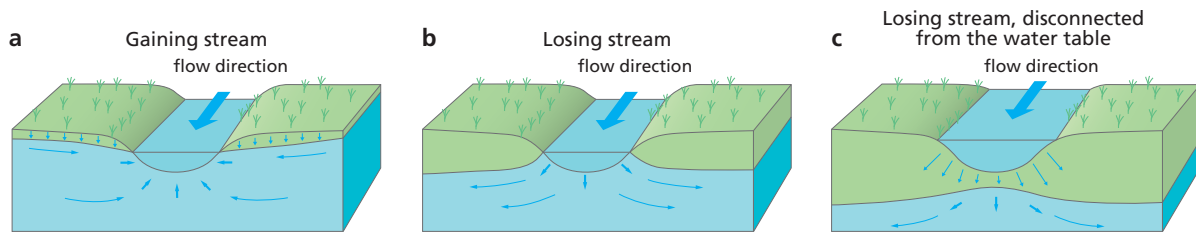
44

45 **1. Introduction**

46 Increasing population, economic growth and changes in diet have dramatically increased the
47 demand for food and water over the last decades (Godfray et al., 2010). To meet increasing
48 demands, irrigated agriculture has expanded into semi-arid areas with limited precipitation
49 and surface water (Siebert et al., 2015). This has greatly intensified the dependence of
50 irrigated crops on groundwater withdrawal (Wada et al., 2012) and caused a steady increase
51 of groundwater depletion rates (Wada and Bierkens, 2019). Recent estimates of current
52 groundwater withdrawal range approximately between 600-1000 km³ yr⁻¹ leading to
53 estimated depletion rates of 150-400 km³ yr⁻¹ (Wada, 2016).

54

55 Groundwater that is pumped comes either out of storage, from reduced groundwater
56 discharge or from reduction of evaporation fed from below by groundwater through capillary
57 rise and/or phreatophytes (Theis, 1940; Alley et al. 1999; Bredehoeft, 2002); Konikow and
58 Leake, 2014). Thus, extensive groundwater pumping not only leads to groundwater depletion
59 (Wada et al., 2010) but also to a reduction in streamflow (Wada et al., 2013; Mukherjee et al.,
60 2019; De Graaf et al., 2019; Jasechko et al., 2021) and desiccation of wetlands and
61 groundwater dependent terrestrial ecosystems (Runhaar et al 1997; Shafroth et al., 2000;
62 Elmore et al 2006; Yin et al 2018). However, the effect of groundwater pumping on
63 groundwater depletion and surface water depletion heavily depends on the nature of the
64 interaction between groundwater and surface water. Limiting ourselves to phreatic
65 groundwater systems and following Winter et al. (1998), a distinction can be made between
66 gaining streams, losing streams and disconnected losing streams, depending on the position
67 of the free groundwater surface with respect to the surface water level and the bottom of the
68 stream (Figure 1). Since groundwater pumping affects groundwater levels, it can move a
69 stream from gaining to losing to disconnected and losing, which, in turn, affects the way
70 that groundwater pumping affects streamflow.



71
 72 *Fig. 1. Groundwater-streamflow interaction: (a) gaining stream; (b) losing stream; (c) losing*
 73 *stream disconnected from the water table; modified from Winter at al. (1998); credit to the*
 74 *United States Geological Survey.*
 75

76 Based on the above, Bierkens and Wada (2019) define two stages of groundwater withdrawal
 77 in phreatic aquifers. In stage 1, groundwater withdrawal is such that the water table remains
 78 connected with the surface water system (Figure 1a, b). Upon pumping, groundwater initially
 79 comes out of storage and groundwater levels decline. However, as groundwater levels decline
 80 around a well, the well attracts more of the recharge that would otherwise end up in the
 81 stream until a new equilibrium is reached where all of the pumped water comes out of
 82 captured streamflow. In a stage 1 withdrawal regime, withdrawal can be considered as
 83 physically stable, where groundwater depletion is limited and groundwater withdrawal
 84 mostly diminishes streamflow and evaporation. Depending on the groundwater level, one
 85 could further distinguish between gaining (Figure 1a) and losing (Figure 1b) streams. This is
 86 important when considering the quality of pumped groundwater as in case of a losing stream
 87 surface water ends up in the well. In a stage 2 withdrawal regime, groundwater withdrawal is
 88 so large that groundwater levels fall below the bottom of the stream (Figure 1c). In that case,
 89 a further decline of the groundwater level hardly increases infiltration from the stream to the
 90 aquifer. Thus, in stage 2, groundwater withdrawal in excess of recharge and (constant) stream
 91 water infiltration is physically unstable and as a result leads to groundwater depletion and
 92 does not impact streamflow further if pumping rates increase.

93
 94 From the above it follows that there is a critical transition between stage 1 and stage 2
 95 groundwater withdrawal that depends on groundwater withdrawal rate. In reality, this
 96 transition is less abrupt. Right after the water table is just below the river bottom, negative
 97 pressure heads occur below the river bed while the soil is fully or partly saturated. Wang et
 98 al. (2015) show experimentally and theoretically that a full disconnection, i.e. the water table
 99 has no impact on the infiltration flux, occurs only when the depth of the groundwater table
 100 below the stream becomes larger than the stream water depth. Another reason that this
 101 transition does not occur abruptly is that multiple surface water bodies in the surroundings of

102 groundwater wells differ in depth depending on stream order and location in the river basin.
103 We also note that that in many regions of the world groundwater is pumped from deeper
104 confined or leaky-confined aquifers (De Graaf et al., 2017). Under confined conditions,
105 groundwaters-streamflow interaction only occurs for the larger rivers that are deep enough to
106 penetrate the confining layer, while in leaky confined aquifers the interactions are more
107 complicated and delayed (Hunt, 2003).

108

109 There are many analytical solutions for calculating the stream depletion rate (SDR), defined
110 as the ratio of the volumetric rate of water abstraction from a stream to groundwater pumping
111 rate. These solutions differ in assumptions about the type of aquifer (unconfined, confined,
112 leaky-confined, multiple aquifers), stream bottom elevation, stream geometry and including
113 additional resistance from the streambed clogging layer or not. We refer to Huang et al.
114 (2018) for an extensive overview of solutions and when to apply them. These analytical
115 solutions typically involve a single well and a single stream, or, using apportionment
116 methods, a single well and stream networks (Zipper et al., 2019), while they consider streams
117 to be connected with the water table. Such analytical solutions could possibly be used for
118 multiple wells using e.g. superposition. However, for more complex situations, with multiple
119 wells, increasing withdrawal rates and streams changing from e.g. connected to disconnected,
120 numerical groundwater models need to be used. These have the disadvantage that they are
121 parameter-greedy, time-consuming to setup and often computationally expensive. Thus,
122 relatively simple analytical tools to assess the effects of extensive multi-well groundwater
123 pumping on groundwater and surface water systems at large are lacking.

124

125 Here, we introduce a simple analytical framework based on a lumped conceptual model of
126 aquifer-stream interaction under pumping. The framework aims to describe at larger scales,
127 i.e. large catchments and/or regional-scale phreatic aquifer systems, to what extent multi-well
128 groundwater withdrawal affects area-average groundwater heads and streamflow. It allows
129 for a shift in the nature of groundwater-surface water interaction, calculates at which critical
130 withdrawal rate such a shift is expected and when it is likely to occur after withdrawal
131 commences. It also provides estimates of streamflow depletion and the partitioning between
132 groundwater storage depletion and reduction in streamflow (capture). We envision that such
133 an analytical framework, when parameterized with parameters and inputs from a more
134 complex global-scale hydrological model, can be used as a screening tool for fast first-order
135 assessments of regional-scale groundwater sustainability, and for supporting hydroeconomic

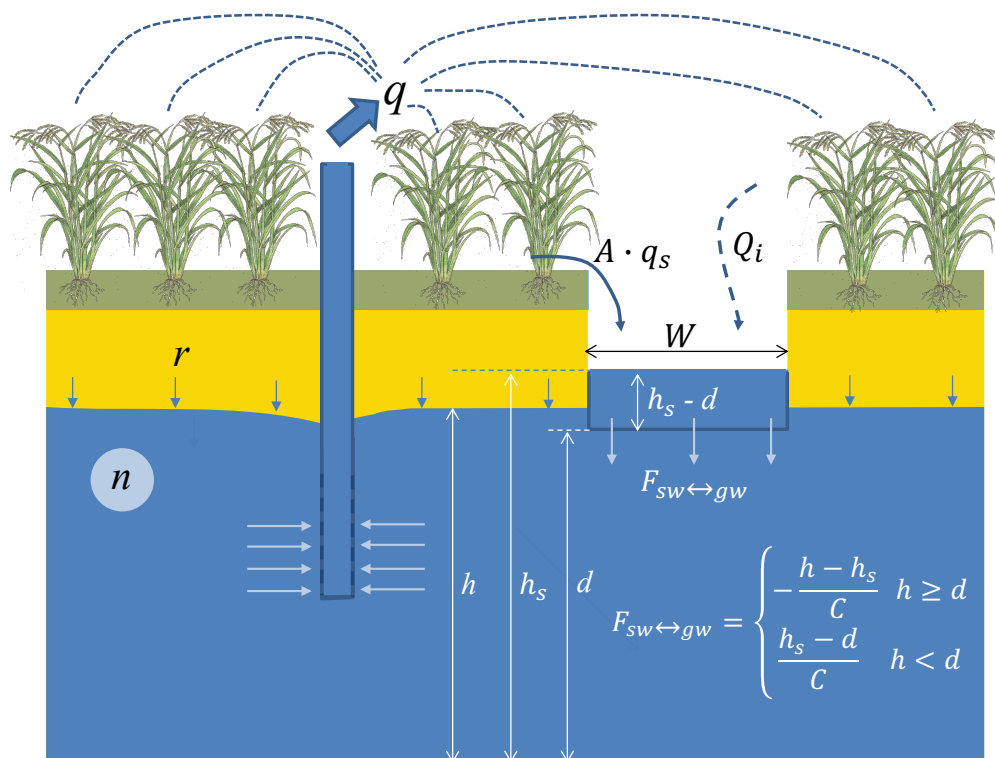
136 models that require simple relationships between large-scale groundwater withdrawal rates
 137 and the evolution of pumping costs and environmental externalities.

138
 139 In the following, we first introduce the lumped conceptual model of large-scale groundwater
 140 pumping with groundwater-surface water interaction. Next, we show its properties with an
 141 extensive sensitivity analysis, followed with a global application of the model using inputs
 142 and parameters from an existing global hydrological model (PCR-GLOBWB 2) and an
 143 evaluation of its performance with estimates from in situ-observations, regional and global
 144 groundwater models and satellites.

145
 146

147 **2. Conceptual model of large-scale groundwater pumping with**
 148 **groundwater-surface water interaction**

149



150
 151 *Figure 2. Conceptual model of groundwater extracted (in this case for irrigation) from an*
 152 *aquifer recharged by diffuse recharge and riverbed infiltration. Symbols are explained in the*
 153 *text.*

154

155 A lumped conceptual hydrogeological model is proposed that allows for the analytical
 156 treatment of area-average large-scale groundwater decline under varying pumping rates, yet
 157 exhibits the properties of surface water-groundwater interaction. Consider a simplified model

158 of a phreatic aquifer subject to groundwater pumping (Figure 2). The volume of groundwater
 159 pumped sums up all the pumping efforts of a large number of land owners that all draw water
 160 from the same aquifer that can be seen as a common pool resource. Recharge consist of
 161 diffuse recharge from precipitation and concentrated recharge from river-bed infiltration,
 162 where river discharge comes from local surface runoff and from inflow from upstream areas
 163 outside the area of interest.

164
 165 Being of lumped nature, the model neglects (lateral) groundwater flow processes within the
 166 aquifer and the mutual influence of multiple wells by treating the aquifer as one pool with a
 167 given specific yield and unknown depth (i.e. physical limits are unknown) subject to pumping
 168 treated as a diffuse sink. The latter is a simplification that represents the effects of hundreds
 169 to thousands of wells of farmers spread more or less evenly across the aquifer. Also, we
 170 assume withdrawal rate, surface runoff and river bed recharge to be constant in time,
 171 neglecting seasonal variations that usually occur due to variation in crop water demand.
 172 These simplifications allow us to represent the change of groundwater level h with a simple
 173 linear differential equation of the total aquifer mass balance:

174
 175
$$n \frac{dh}{dt} = r + F_{gw \leftrightarrow sw}(h) - q \quad (1)$$

176 With

177 h : groundwater head (m)

178 n : specific yield (-)

179 q : pumping rate per area ($\text{m}^3 \text{m}^{-2} \text{yr}^{-1}$)

180 $F_{gw \leftrightarrow sw}$: surface water infiltration (or drainage) flux density ($\text{m}^3 \text{m}^{-2} \text{yr}^{-1}$)

181

182 The groundwater - surface water flux is modelled as follows:

183
$$F_{gw \leftrightarrow sw}(h) = \begin{cases} -\frac{h-h_s}{c} & h \geq d \\ \frac{h_s-d}{c} & h < d \end{cases} \quad (2)$$

184 with h_s is the surface water level and d the elevation of the bottom of the water course. The
 185 parameter C is a drainage resistance (yr) which pools together all the parameters of surface-
 186 water groundwater interaction, i.e. the density or area fraction of surface waters, surface
 187 water geometry and river/lake-bed conductance and the hydraulic conductivity of the aquifer.
 188 Equation (2) is also used to describe groundwater-surface water interaction in numerical
 189 groundwater such as MODFLOW (McDonald and Harbaugh, 2005), as well as in several

190 large-scale hydrological models (Döll et al., 2014; Sutanudjaja et al., 2018). This is a
 191 simplification of the true interaction where in case of a detachment of the groundwater level
 192 and the river bed ($h < d$) negative pressure heads can occur below the river bed and Equation
 193 (2) may underestimate the river bed infiltration (Brunner et al., 2010). However, this latter
 194 study also shows that errors remain within 5% in case the surface water is deep enough (> 1
 195 m). Equation (2) provides a critical transition in terms of the effect of pumping on the
 196 hydrological system. As long as the groundwater level is above the bottom of the surface
 197 water network, the groundwater-surface water flux acts as a negative feedback on
 198 groundwater level decline, at the expense of surface water decline. As the water table falls
 199 below the bottom elevation (only possible if pumping rate q is large enough; see hereafter),
 200 surface water decline stops and progressive groundwater decline sets in.

201

202 The surface water level itself is a variable which is related to the surface water discharge Q
 203 ($\text{m}^3 \text{y}^{-1}$) and the groundwater level as follows:

204

$$205 \quad Q = Wv(h_s - d) = Q_i + q_s A - F_{gw \leftrightarrow sw}(h)A \quad (3)$$

206 with

207 A : The area over the (sub-)aquifer considered (m^2)

208 q_s : surface runoff (m yr^{-1})

209 Q_i : influx of surface water from upstream ($\text{m}^3 \text{yr}^{-1}$)

210 W : Stream width (m)

211 d : Bottom elevation stream (m)

212 v : Stream flow velocity (m yr^{-1})

213

214 The influx Q_i is added to account for aquifers in dry climates where the surface water system
 215 is fed by wetter upstream areas, e.g. mountain areas. The surface runoff q_s (including shallow
 216 subsurface storm runoff) also supplements the streamflow. Equation (3) lumps the
 217 streamflow system overlying the phreatic aquifer system with a representative discharge,
 218 water height, flow velocity and stream width taken constant in time. Equations (1)-(3)
 219 together describe the coupled surface water-groundwater system where all parameters and
 220 inputs remain constant with time and groundwater head h and surface water levels h_s change
 221 over time as a result of groundwater pumping only.

222

223 In Appendix A expressions are derived for the following properties of the coupled system:

224 q_{crit} Critical pumping rate ($m^3 m^{-2} yr^{-1}$) above which the groundwater level becomes
225 disconnected from the stream.

226 t_{crit} Critical time (years after start of withdrawal) at which the groundwater level
227 becomes disconnected from the stream, i.e. $h < h_s$.

228 $h(t)$ Groundwater head (m) over time

229 $h(\infty)$ Equilibrium groundwater head (m) at $t=\infty$ that only occurs in case $q \leq q_{crit}$

230 $h_s(t)$ Surface water level (m) over time.

231 $h_s(\infty)$ Equilibrium surface water level (m), which is different when $q \leq q_{crit}$ than when
232 $q > q_{crit}$.

233 $Q(t)$ Surface water discharge ($m^3 yr^{-1}$) over time.

234 $Q(\infty)$ Equilibrium surface water discharge ($m^3 yr^{-1}$), which is different when $q \leq q_{crit}$
235 than when $q > q_{crit}$.

236 $q_{stor}(t)$ Part of the pumped groundwater that comes out of storage, which is different
237 when $q \leq q_{crit}$ than when $q > q_{crit}$.

238 $q_{cap}(t)$ Part of the pumped groundwater that comes from capture (reduction in
239 streamflow), which is different when $q \leq q_{crit}$ than when $q > q_{crit}$.

240

241 Table 1 provides an overview of the mathematical expressions derived for each of these
242 properties in Appendix A. The left column shows the stable regime where upon
243 commencement of pumping after some time an equilibrium is reached with equilibrium
244 groundwater levels $h(\infty)$, streamflow $Q(\infty)$ and surface water level h_s . The middle and right
245 columns show the results of unstable groundwater withdrawal. The behavior of $h(t)$, $Q(t)$ $h_s(t)$
246 follows that of the stable regime until time $t = t_{crit}$ when the groundwater level drops below
247 the bottom of the surface water. After this time the groundwater level $h(t)$ shows a persistent
248 decline and surface water level $h_s(t)$, streamflow $Q(t)$ and the fraction of water pumped from
249 capture become constant.

250

251

252

253

254

255

256 *Table 1. Overview of derived expressions for groundwater properties used in this paper*

$\alpha = \frac{Q_i C + q_s A C + W v d C}{W v C + A} \quad \beta = \frac{A}{W v C + A} \quad q_{crit} = r + \frac{Q_i + q_s A}{W v C + A}$		
$q \leq q_{crit}$	$q > q_{crit}$	
	$t_{crit} = \frac{nC}{1-\beta} \ln\left(\frac{qC}{qC - (rC + \alpha) + d(1-\beta)}\right)$	
	$t \leq t_{crit} (h \geq d)$	$t > t_{crit} (h < d)$
$h(t) = \frac{rC + \alpha}{1-\beta} - \left(\frac{qC}{1-\beta}\right) \left[1 - e^{-\left(\frac{1-\beta}{nC}\right)t}\right]$ $h(\infty) = \frac{rC + \alpha - qC}{1-\beta}$	$h(t) = \frac{rC + \alpha}{1-\beta} - \left(\frac{qC}{1-\beta}\right) \left[1 - e^{-\left(\frac{1-\beta}{nC}\right)t}\right]$	$h(t) = d + \left[\frac{r-q}{n} + \frac{(Q_i + q_s A)}{n(WvC + A)}\right] (t - t_{crit})$
$h_s(t) = \alpha + \beta h(t)$ $h_s(\infty) = \alpha + \frac{\beta(rC + \alpha - qC)}{1-\beta}$	$h_s(t) = \alpha + \beta h(t)$	$h_s = d + \frac{(Q_i + q_s A)C}{WvC + A}$
$Q(t) = Q_i + q_s A - \frac{A\alpha}{C} + \frac{A(1-\beta)}{C} h(t)$ $Q(\infty) = Q_i + (q_s + r - q)A$	$Q(t) = Q_i + q_s A - \frac{A\alpha}{C} + \frac{A(1-\beta)}{C} h(t)$	$Q = \frac{(Q_i + q_s A)WvC}{WvC + A}$
$q_{stor} = q e^{-\left(\frac{1-\beta}{nC}\right)t}$ $q_{cap} = q \left(1 - e^{-\left(\frac{1-\beta}{nC}\right)t}\right)$	$q_{stor} = q e^{-\left(\frac{1-\beta}{nC}\right)t}$ $q_{cap} = q \left(1 - e^{-\left(\frac{1-\beta}{nC}\right)t}\right)$	$q_{stor} = q - \left(r + \frac{(Q_i + q_s A)}{(WvC + A)}\right)$ $q_{cap} = r + \frac{(Q_i + q_s A)}{(WvC + A)}$

257

258

259 **3. Local sensitivity analyses**

260 Figure 3 shows the results of a sensitivity analysis for the critical withdrawal rate q_{crit} and the
 261 critical time until the water table disconnects from the stream t_{crit} . For the stable regime
 262 ($q \leq q_{crit}$) it shows the change in groundwater level at equilibrium $dh=h(0)-h(\infty)$, the change
 263 in streamflow at equilibrium $dQ = Q(0)-Q(\infty)$ and the e -folding time $t_{ef} = nC/(1-\beta)$ of
 264 reaching the equilibrium after the commencement of pumping. For the unstable regime, we
 265 show the decline rate of the groundwater level dh/dt , the (constant) streamflow depletion dQ
 266 and the constant fraction of capture ($f_{cap} = q_{cap}/q$). We stress that our sensitivity analysis is far
 267 from exhaustive (global) and that sensitivity plots are shown to provide a general feel of the
 268 behavior of the model and to show relationships between parameters and outputs that are of

269 interest to show. Unless they are varied on one of the axes, the parameter values used are the
 270 reference values denoted in Table 2.

271

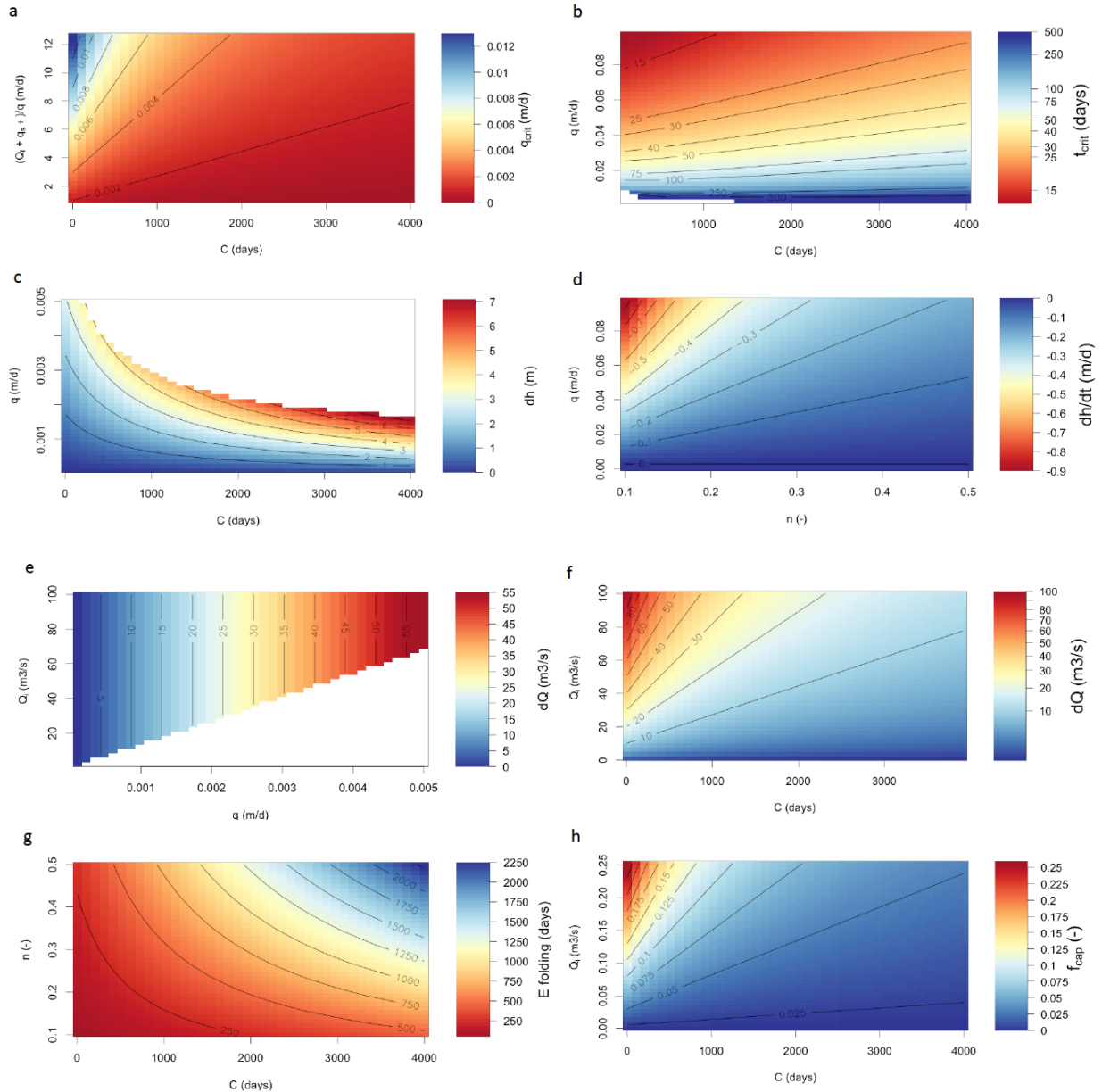
272 *Table 2. Reference parameter values used in sensitivity analyses.*

Parameter	Value
Surface water system	
A	1000 km ²
q_s	0.001 m d ⁻¹
Q_i	50 m ³ s ⁻¹
d	95 m
W	20 m
v	1 m s ⁻¹
Hydrogeology	
C	1000 d
n	0.3
r	0.001 m d ⁻¹

273

274

275 Figure 3a shows that the critical withdrawal rate increases with the relative abundance of
 276 surface water due to upstream inflow and runoff and decreases with a decreased strength of
 277 the surface water-groundwater interaction (increased value of C). For stable withdrawal rates
 278 we see the largest equilibrium groundwater level declines with increased pumping rates and
 279 decreased strength of surface water-groundwater interaction, i.e. decreased capture (Figure
 280 3c). Figure 3e shows that the equilibrium reduction in streamflow to be proportional to
 281 groundwater withdrawal rate as expected, but to depend only mildly on the upstream inflow.
 282 The latter is caused by the two-way interaction between surface water and groundwater:
 283 increasing inflow for a given withdrawal rate reduces groundwater level decline, which in
 284 turn limits the loss of surface water to the groundwater. As follows from the expression
 285 $t_{ef} = nC/(1 - \beta)$, the time to equilibrium (Fig. 3g) , i.e. the time until the pumped
 286 groundwater originates completely from capture and no further storage changes occur, is
 287 proportional to the resistance value C and the specific yield, where the degree of
 288 proportionality depends on the surface water properties. Figure 3g also shows that the time to
 289 full capture can be very large, up to several decades.



290

291

292 *Figure 3. Results of the sensitivity analyses showing parameter dependence of q_{crit} (a) and*
 293 *t_{crit} (b); variables under stable withdrawal: $dh=h(0)-h(\infty)$ (c), $dQ=Q(0)-Q(\infty)$ (e),*
 294 *$t_{ef} = nC/(1 - \beta)$ (g) t_{crit} and variables under unstable withdrawal and $t > t_{crit}$: dh/dt (d), dQ*
 295 *(f) and $f_{cap} = q_{cap}/q$.*

296

297 Figures 3b-h (right column) provides sensitivity plots of relevant variables in the unstable
 298 regime. Figure 3b shows that under the unstable regime, the time t_{crit} to a transition from a
 299 connected to a non-connected groundwater table decreases with withdrawal rate, but slightly
 300 increases with C . The latter seems counter-intuitive at first, because a larger value of C means
 301 reduced surface water contribution and therefore likely larger groundwater level decline rates
 302 and smaller values of t_{crit} . The equation for $h(t)$ in Table 1 (Equation A10 in the appendix)
 303 shows that this is indeed the case for early times but that for later times the decline rates are

304 reduced by a larger value of C in the term factor $(1 - \beta)/nC$ in the exponential. Figures 3d-h
305 show sensitivity plots for $t > t_{crit}$ ($h < d$), i.e. groundwater levels are disconnected from the
306 surface water, groundwater is persistently taken out of storage and the capture becomes
307 constant. As expected, the groundwater level decline rates (Figure 3d) are proportional to
308 withdrawal rates and inversely proportional to specific yield. The final reduction in
309 streamflow (Figure 3f) for $t > t_{crit}$ decreases with the value of C (limited surface water-
310 groundwater interaction), while the availability of surface water is important for smaller
311 values of C . Here, a larger inflow leads to larger losses because losses are proportional to the
312 surface water level which increases with inflow. Figure 3h resembles that of Figure 3f
313 because apart from the constant recharge, the fraction of capture is proportional to the
314 streamflow reduction which ends up in the pumped groundwater

315
316

317 **4. Global-scale application**

318 ***Global parameterization***

319 We applied the analytical framework to the global scale at 5 arc-minute resolution
320 (approximately 10 km at the equator) by obtaining parameters and inputs from the global
321 hydrology and water resources model PCR-GLOBWB 2 (Sutanudjaja et al., 2018, See Table
322 3 and Figures S1-S9 in the Supplement). For the flux densities q , q_s , r , the discharge Q_i and
323 the velocity v we used the average values over the period 2000-2015. Note that for an
324 application of the analytical framework at a cell-by-cell basis, the reduction in streamflow dQ
325 in a given cell should be accounted for by reducing the inflow Q_i to the downstream cell.
326 However, by using as inflow Q_i the upstream discharge from a PCR-GLOBWB simulation
327 that includes human water use, upstream withdrawals from surface water and groundwater
328 are already accounted for. Note that they would also be implicitly included in case an
329 observation-based streamflow dataset (e.g., Barbarossa et al., 2019) would have been used for
330 Q_i . The groundwater-surface water interaction parameter C is determined from the
331 characteristic response time J of the groundwater reservoir in PCR-GLOBWB 2, which is
332 based on the drainage theory of Kraijenhoff-van de Leur (1958). From this solution and
333 Equation (2) it can be shown that $C=J/n$ (see Appendix B). Since the variables q_{crit} and t_{crit}
334 depend heavily on the value of C we have also included the dataset of groundwater response
335 time published by Cuthbert et al. (2019) to calculate the C value.

336
337

338 *Table 3. Parameter and input values used in global-scale analyses at 5 arc-minute cells (~10*
 339 *km ar the equator). All inputs obtained from PCR-GLOBWB 2 (Sutanudjaja et al., 2018),*
 340 *except the C value obtained from PCR-GLOBWB and from Cuthbert et al. (2018); a input*
 341 *variables averaged over the period 2000-2015.*

Parameter	Value
Surface water system	
A	Cell area 5 arc-minute cells (m ²)
q_s	Sum of surface runoff and interflow (m d ⁻¹) of a cell
Q_i	Upstream discharge of a cell (m ³ d ⁻¹)
d	Stream elevation (m) based on bankfull discharge
W	Stream width (m) based on bankfull discharge
v	Calculated from bankfull discharge and stream depth (m d ⁻¹) at Bankfull discharge, assuming v to be dependent on terrain slope only.
Hydrogeology	
C	$C = J/n$ (d), with J the characteristic response time of the groundwater reservoir (Sutanudjaja et al. 2018) or groundwater response times from Cuthbert et al. (2019).
n	Porosity values (-) from the groundwater reservoir in PCR-GLOBWB.
r	Net recharge (recharge minus capillary rise) (m d ⁻¹).
q	Pumping rate (m d ⁻¹).

342

343 **Global results**

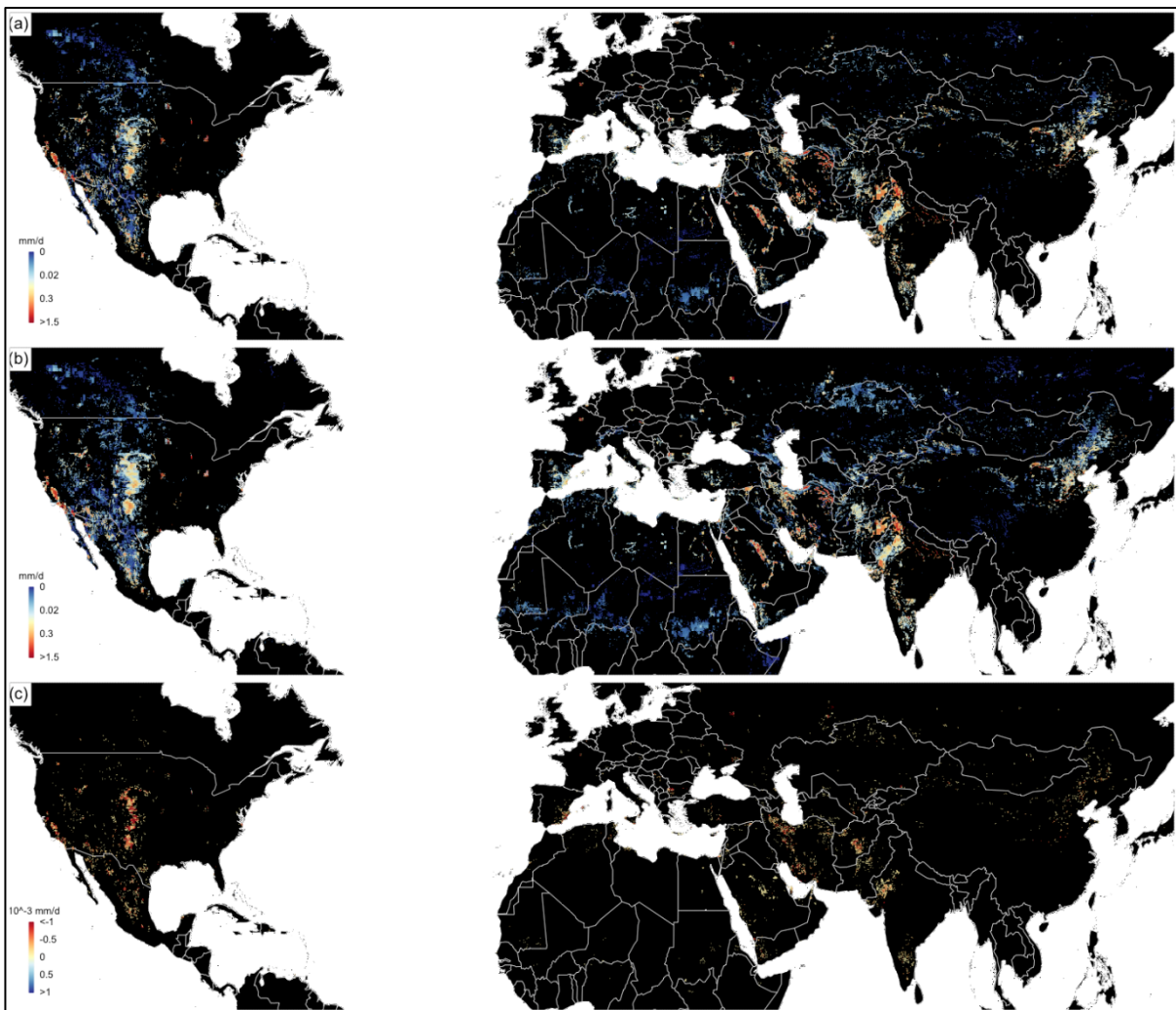
344 Figure 4 shows the groundwater depletion rates $q-q_{crit}$ for the areas with unstable
 345 groundwater withdrawal. The resulting patterns are similar to those calculated from previous
 346 global studies (Wada et al., 2012; Döll et al., 2014) and show the well-known hotspots of the
 347 world. Total depletion rates in Figure 4 are 158 km³ yr⁻¹ (a) and 166 km³ yr⁻¹ (b), which are in
 348 the range of previous studies, e.g., 234 km³ yr⁻¹ (Wada et al., 2012; year 2000), 171 km³ yr⁻¹
 349 (Sutanudjaja et al., 2018; 2000-2015) and 113 km³ yr⁻¹ (Döll et al., 2014; 2000-2009).

350

351 The similarity of the groundwater depletion estimates with those obtained from global
 352 hydrological models can be explained by the the fact that the way the groundwater-surface
 353 water system is modelled in Figure 1 is similar to how the groundwater reservoirs and their
 354 interaction with surface water have been implemented in global hydrological models such as
 355 PCR-GLOBWB (De Graaf et al., 2015) and WGHM (Döll et al., 2014) (see also Appendix
 356 B). Since the groundwater dynamics of latter models are (piece-wise) linear and groundwater
 357 recharge in our model is applied directly in Equation (1) – i.e. the non-linear responses of the
 358 soil system to precipitation and evaporation is bypassed -, forcing our model with average
 359 fluxes r , q , Q_i and q_s and using the parameter J from PCR-GLOBWB yields almost the same
 360 depletion rates as from the time varying model simulations with PCR-GLOBWB. The small

361 difference between our estimate ($158 \text{ km}^3 \text{ yr}^{-1}$) and the value from PCR-GLOBWB 2
 362 (Sutanudjaja et al., 2018) ($171 \text{ km}^3 \text{ yr}^{-1}$) is explained by a resulting non-linearity not
 363 accounted for: during dry periods some of the streams in the PCR-GLOBWB run dry and do
 364 not contribute to the concentrated recharge flux. It should be noted that our results are
 365 obtained at only a fraction of the computational costs of global hydrological models: a few
 366 minutes at a single PC compared to 2 days on a 48-core machine with PCR-GLOBWB at 5
 367 arc-minutes. Thus, the sensitivity to changing pumping rates or changes in recharge under
 368 climate change can be quickly evaluated.

369

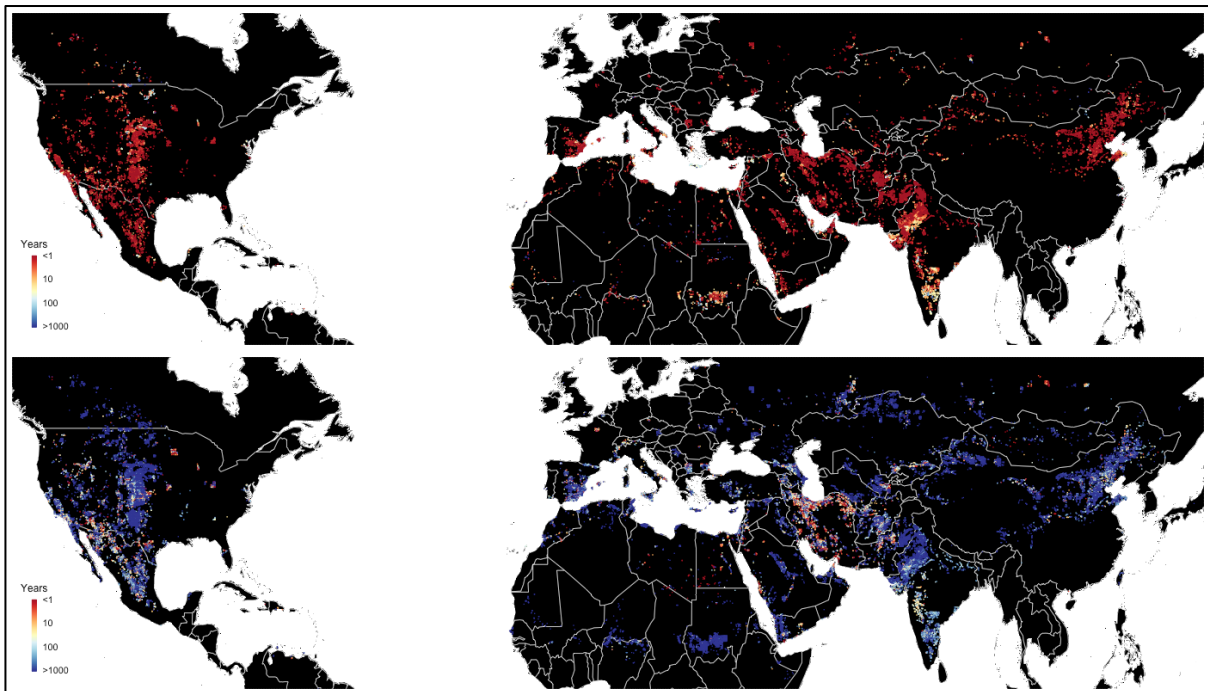


370
 371 *Figure 4. Average groundwater depletion rates ($q - q_{crit}$) over 2000-2015 at 5 arc-minute*
 372 *resolution calculated with the data from Table 2. (a) using C-values from Sutanudjaja et al.*
 373 *(2018); (b) using C-values based on Cuthbert et al. (2019); (c) difference map $a - b$.*
 374

375 Figure 5 shows the time to critical transition t_{crit} from both datasets. It is quite striking that,
 376 although the depletion rates are rather similar between datasets (Figure 4), the critical
 377 transition times are much larger for the Cuthbert et al. (2018) dataset. These differences can

378 even add up to 2-3 orders of magnitude, which is extremely large. The reason is that the
 379 characteristic response times based on Cuthbert et al. (2018) are much larger (also up to 2-3
 380 orders of magnitude) than those based on PCR-GLOBWB. Since the e-folding time in the
 381 stable regime is close to proportional to the C -value (e.g., Figure 3g), this is also true for the
 382 critical transition time. The very large differences in response times between these two
 383 datasets reveals that our method is only as good as its inputs and that critical transition times
 384 and times to full capture calculated with our approach should be interpreted with care and as
 385 order of magnitude estimates at best.

386

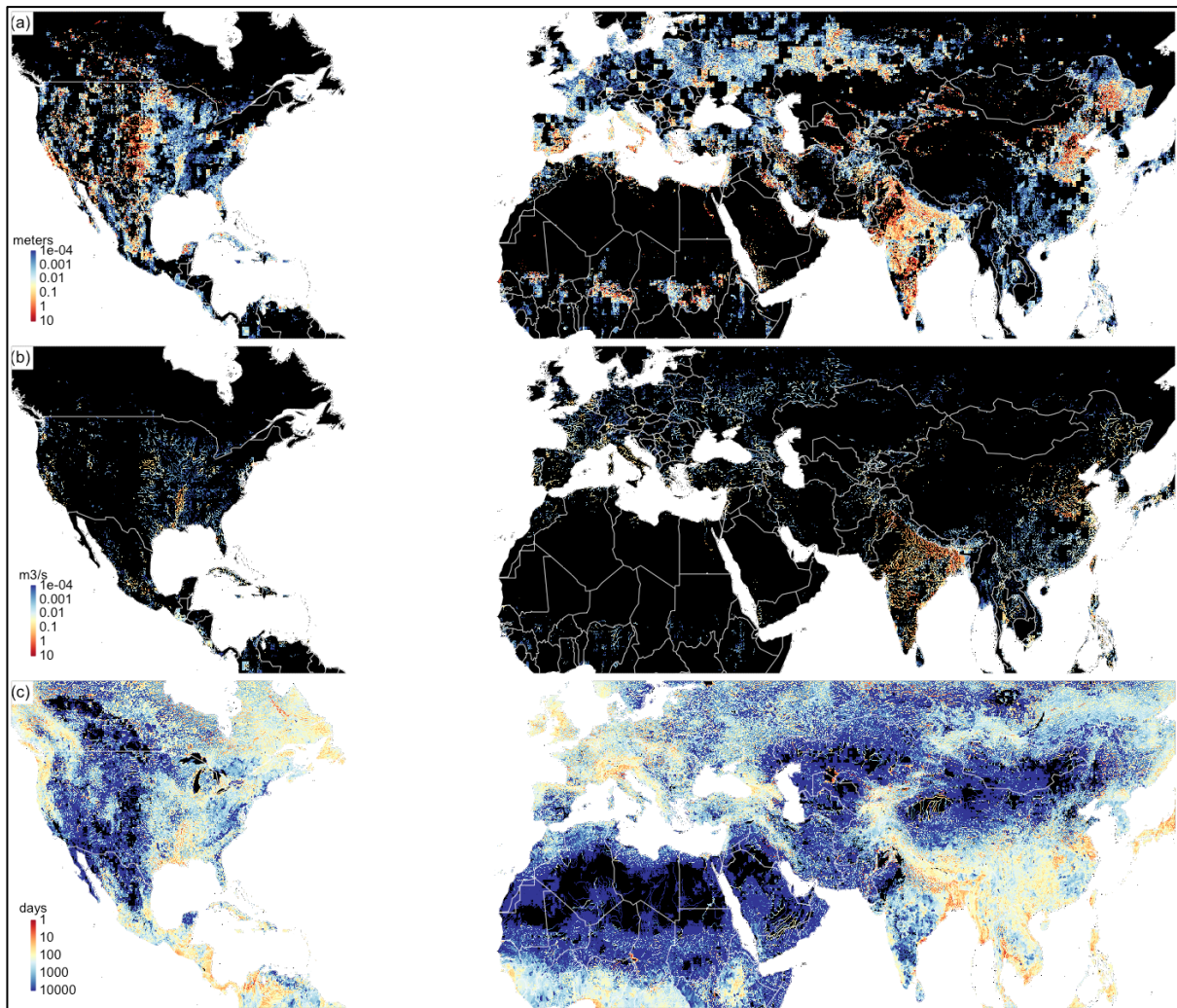


387
 388 *Figure 5. Critical transition times (Critical time at which the groundwater level becomes*
 389 *disconnected from the stream after start of pumping, i.e. $h < h_s$ in case $q > q_{crit}$) calculated*
 390 *with the data from Table 1. The top figure uses C -values from Sutanudjaja et al. (2018) and*
 391 *the lower figure from Cuthbert et al. (2019).*

392

393 To further explore the global impacts of groundwater withdrawal we calculated relevant
 394 output variables for the areas that have been identified as subject to stable groundwater
 395 withdrawal ($q \leq q_{crit}$; Figure 6) and unstable withdrawal ($q > q_{crit}$; Figure 7). Figure 6a
 396 shows the equilibrium water table decline from stable groundwater withdrawal. We see the
 397 largest declines occurring in areas with larger groundwater withdrawals, which are often
 398 close to the depletion areas (Figure 4) and coincide with regions with limited surface water
 399 occurrence due to a semi-arid climate (higher C -values). In contrast, the equilibrium decline
 400 in streamflow (Figure 6b) is focused in areas with significant groundwater withdrawal and

401 higher surface water densities (low C -values), which are those areas that have a more semi-
 402 humid climate where both groundwater and surface water use are present. These are also the
 403 areas with relatively short times to equilibrium (Figure 6c).

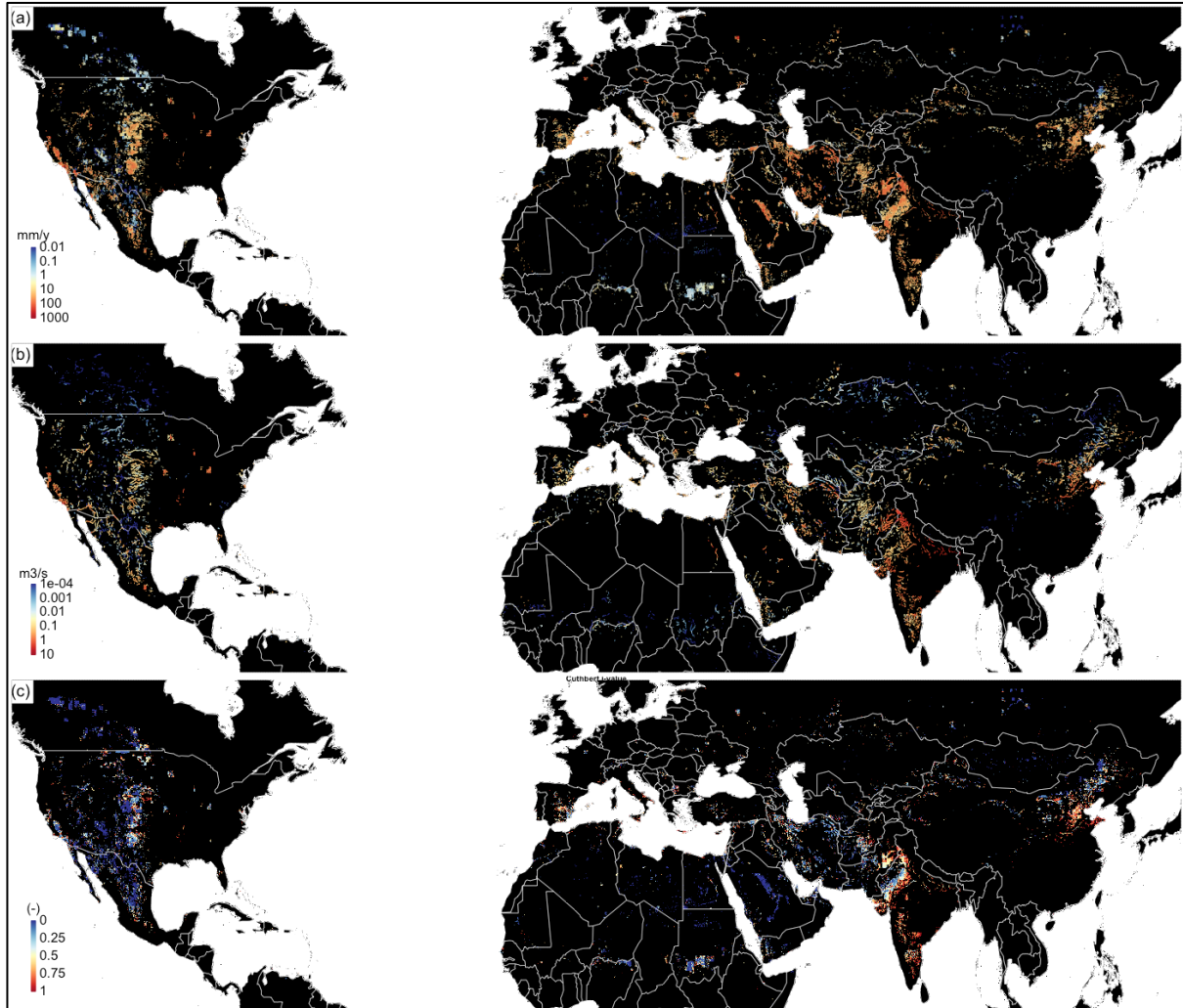


404
 405 *Figure 6. Results for the areas with stable withdrawal rates ($q \leq q_{crit}$); (a) equilibrium*
 406 *groundwater level decline (m); (b) equilibrium reduction of discharge ($m^3 s^{-1}$); (c) e-folding*
 407 *time to complete capture (d); black areas are areas without groundwater withdrawal, with*
 408 *unstable groundwater withdrawal or negligible values ($< 10^{-4}$).*

409
 410 As expected, the groundwater decline rates under unstable withdrawal (Figure 7a) mirror the
 411 depletion rates (Figure 4). Estimates based on piezometers for major depleting areas are in
 412 the order of 0.4-1.0 m yr⁻¹ in Southern California and the Southern High Plains aquifer
 413 (Scanlon et al., 2012) and 0.1-1.0 m yr⁻¹ in the Gangetic plain (MacDonald et al., 2016). Our
 414 estimates are in the lower end of those observed ranges, which could be partly explained by
 415 the fact that, particularly in the U.S., groundwater withdrawal is from semi-confined aquifers,
 416 leading to a larger head decline per volume out of storage than follows from the specific
 417 yields used in our conceptual model. The largest change in streamflow and the highest

418 fraction of capture are found in areas where groundwater depletion coincides with the
419 presence of surface water, e.g. such as the Northern and Eastern part of the Ogallala aquifer,
420 the Indus basin and southern India.

421



422

423 *Figure 7. Results for the areas with unstable withdrawal rates ($q > q_{crit}$); (a) groundwater*
424 *level decline rate (mm yr^{-1}); (b) equilibrium reduction of discharge ($\text{m}^3 \text{s}^{-1}$); (c) fraction of*
425 *capture (-); black areas are areas without groundwater withdrawal, with stable groundwater*
426 *withdrawal or with negligible values ($< 10^{-4}$).*

427

428 ***Sensitivity and evaluation of global results***

429 Critical parameters that determine the stream-aquifer interaction and hence many of the
430 outputs shown in Figures 4-7 are the stream-aquifer resistance parameter C and the stream
431 bottom elevation d . We performed a local sensitivity analysis by changing the parameters C
432 and $d \pm 10\%$ around their current values (Figures S3 and S6 in Supplement) and calculated the
433 relative change in the output per unit relative change in parameters C and d . The results
434 (Supplementary Table S1) reveal that for most outputs the sensitivity to C and d is limited

435 (below unity). A notable exception is the sensitivity of t_{crit} to d which can be quite large,
436 particularly for the lower values of C from Sutanudjaja et al. (2018). From the sensitivity
437 analysis we conclude that the global results are relatively robust to changes in the parameters
438 C and d , except for the critical time to stream-aquifer disconnection which is sensitive to d
439 and to a lesser extent to C .

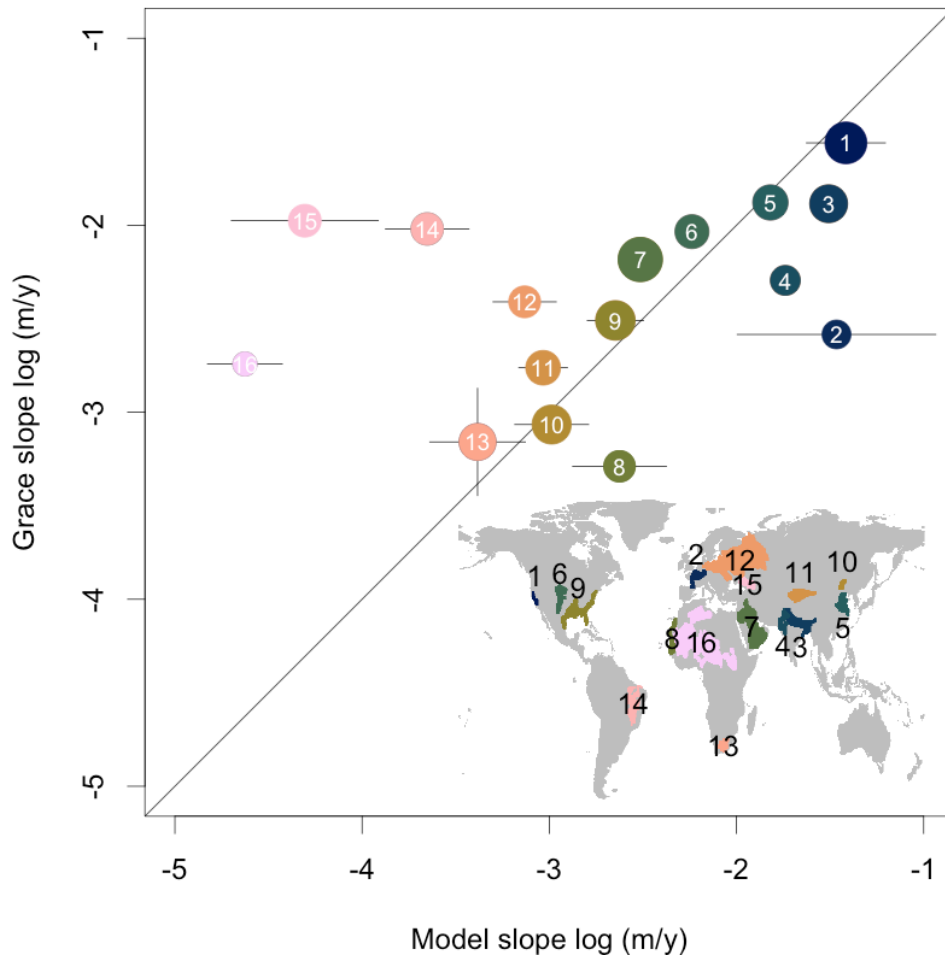
440

441 To evaluate our global results we compare these with observations and model results at
442 various scales, working from large to smaller scales (both in extent and resolution). These
443 include: aquifer average storage change from the Gravity Recovery and Climate Experiment
444 (GRACE) satellite, global-scale groundwater and streamflow depletion estimates from a
445 global groundwater model (De Graaf et al., 2019), continental-scale (conterminous U.S.)
446 groundwater and streamflow depletion estimates from Parflow-CLM (Condon and Maxwell,
447 2019) and groundwater flow and streamflow decline rates for the Republican River Basin
448 based on in-situ observations (Wen and Chen, 2006; McGuire, 2017).

449

450 From the results in Figure 4a (with C from Sutanudjaja et al., 2018; assuming $q > q_{crit}$ and
451 $t > t_{crit}$) we computed average depletion rates of the world's major aquifers subject to
452 depletion (following Richey et al., 2015) and compared these with average trends in total
453 water storage (TWS) from GRACE (Gravity Recovery and Climate Experiment) gravity
454 anomalies over the period 2003-2015 (Figure 8). We used the JPL GRACE Mascon product
455 RL05M (Wiese, 2015; Watkins et al., 2015; Wiese et al., 2016). We did not correct TWS for
456 changes in other hydrological stores, assuming the latter to be approximately constant over a
457 13-year period in semi-arid areas with limited surface water and TWS trends to mainly reflect
458 groundwater depletion. Figure 8 shows that the estimated depletion rates are reasonably
459 consistent with the GRACE estimates, particularly for the known hotspot aquifers with the
460 largest depletion. Notable exceptions are an overestimation of the depletion rate in the Paris
461 Basin and underestimation of depletion rates of the Maranhao Basin, the North Caucasus
462 Basin and the North African Aquifer Systems. These differences may be caused by errors in
463 withdrawal data from PCR-GLOBWB 2 (Supplementary Figure S9), errors in streamflow
464 leakage and errors that result from not correcting the GRACE products for possible secular
465 trends in other hydrological stores. A notable effect could be that by assuming aquifers to be
466 unconfined, we overestimate the leakage from surface water to groundwater in pumped
467 confined aquifers, leading to an underestimation of depletion rates. It should also be noted
468 however that the aquifers whose depletion rates are underestimated have estimated GRACE

469 trends between 1-10 mm yr⁻¹, just above the accuracy limit of GRACE TWS trends (viz.
 470 Richey et al., 2015).



471
 472

473 *Figure 8. Comparison of depletion rates in Figure 4a for major groundwater basins with*
 474 *average depletion rates from GRACE (m yr⁻¹). Size of the circles is proportional to aquifer*
 475 *area; crosses are standard errors in estimated mean aquifer trends; 1: Central Valley*
 476 *(California); 2: Paris Basin; 3 Ganges-Brahmaputra Basin; 4: Indus Basin; 5: North China*
 477 *Plane; 6. Ogallala (High Plains) Aquifer; 7. Arabian Aquifer System; 8: Senegalo-*
 478 *Mauretanian Basin; 9: Atlantic and Gulf Coastal Plains Aquifer; 10: Song-Liao Basin; 11:*
 479 *Tarim basin; 12; Russian Platform Basins; 13: Karoo Bason; 14: Maranhao Basin; 15:*
 480 *North Caucasus Basin; 16: North African Aquifer Systems.*

481

482 At the global scale, we compared the head decline rate (mm d⁻¹) calculated with the analytical
 483 framework with average decline rates over the period 2000-2015 as obtained from the global
 484 groundwater model of De Graaf et al (2019). Note that we restricted this comparison to the
 485 areas with unstable withdrawal rates ($q > q_{crit}$, $t > t_{crit}$). The results shown in Figure S10 show
 486 that the patterns of high and low values of the two estimates are similar, but that the
 487 estimated decline rates from our analytical framework are larger than those estimated by De

488 Graaf et al. (2019). The most likely cause for the larger values in our approach is that it
489 neglects the impact of lateral flow (across cell boundaries) or that the J -value of PCR-
490 GLOBWB used to calculate the C parameter (see Appendix B) is too large so that leakage
491 from the streams is underestimated. Comparison of the stream depletion estimates from the
492 analytical framework (See Supplement Fig. S11; assuming $q > q_{crit}$, $t > t_{crit}$ or $q < q_{crit}$, $t \gg t_{ef}$)
493 shows similar patterns to that of De Graaf et al. (2019), but also slightly larger values. Thus,
494 the most likely cause for the larger depletion values of our analytical framework (Figure S10)
495 is the neglect of lateral flow between cells.

496
497 At the continental scale, we compared groundwater storage changes (m) and stream depletion
498 (% of mean annual flow) across part of the conterminous U.S. obtained from a ParFlow-CLM
499 model (Condon and Maxwell, 2019) with the global estimates from our analytical
500 framework. ParFlow simulates coupled groundwater and surface water flow by solving the
501 3D Richards' equation and the diffusive wave equation respectively, while the community
502 land model CLM includes land surface processes such as evaporation, plant water use, snow
503 accumulation and snow melt. Condon and Maxwell (2019) calculate the total effects of
504 pumping from the predevelopment stage (1900 until 2008), while our global results are based
505 on the average withdrawal rates for the period 2000-2015. To make our results comparable
506 with those of Condon and Maxwell (2019), we took their reported total storage loss of ~ 1000
507 km^3 since 1900 and determined the period length for which the total groundwater withdrawn
508 based on Sutanudjaja et al (2018) across the U.S. approximately equals 1000 km^3 . This
509 resulted in the period 1965-2015. We subsequently recalculated the global maps using the
510 average groundwater withdrawal rate over 1965-2015 from Sutanudjaja et al. (2018).

511 The results are shown in the Supplementary Figures S12 (for $q > q_{crit}$, $t > t_{crit}$) and S13
512 ($q > q_{crit}$, $t > t_{crit}$ or $q < q_{crit}$, $t \gg t_{ef}$). Figure S12 shows again that the analytical approach
513 yields larger depletion estimates than ParFlow, but the results are more similar than with the
514 global model of De Graaf et al (2019). It is speculative at best to explain why the results of
515 Condon and Maxwell (2019) are more similar. One possible explanation may be that the
516 overestimation of decline rates due to ignoring lateral flow between cells in our approach is
517 partly offset by the neglect of headwater streams falling dry under continuous pumping. This
518 effect is included in ParFlow-CLM, which results in larger head decline rates that are closer
519 to ours. The global groundwater model of De Graaf et al (2019) does not include this effect
520 as streams in this model remain water carrying, even if the groundwater level drops below the
521 stream bottom elevation.

522 Figure S13 (top) shows the percentage reduction of streamflow by groundwater pumping
523 since predevelopment as calculated by ParFlow-CLM and Figure S13 (bottom) the
524 estimates based on the analytical framework. We show both maps for reference in the
525 Supplement, but it turns out that comparing the streamflow reduction of the analytical
526 framework with that of ParFlow-CLM is inhibited by differences in model output and
527 presentation. The ParFlow-CLM results represent cumulative dQ as fraction of Q , whereas
528 the results from the analytical framework represent marginal dQ as a fraction of Q , which
529 makes the results only comparable for the headwater catchments. Also, the difficulty of
530 comparison due to the resolution gap (ParFlow-CLM: 1 km; analytical framework: 5
531 arcminutes ~ 10 km) is exacerbated due to the different map formats (vector and vs. raster).
532 Therefore, we refrain from further comments and show the maps as they are.

533

534 At the basin scale, we compared our global results with trends in groundwater head decline
535 and streamflow decline as obtained from observations of groundwater levels and surface
536 water discharge in the Republican River Basin (U.S.A.). The Republican Basin runs through
537 the northern part of the High Plains Aquifer system which is heavily influenced by
538 groundwater withdrawal. We used data from a study by Wen and Chen (2006) that estimated
539 trends in streamflow over the period 1950-2003 for 24 gauging stations spread across the
540 Republican river and its tributaries. The trends were adjusted for possible trends in
541 precipitation and are therefore assumed to only reflect a decrease in streamflow as a result of
542 groundwater pumping. This resulted in 18 out of the 24 stations with significant negative
543 trends. Wen and Chen (2006) also provide groundwater level observations from three wells
544 with filters in the Ogallala formation at three location positioned in three representative
545 locations in the Republican Basin. We used the analytical framework with global parameters
546 (Table 3) but with the average values of q , q_s , r , Q_i over the period 1960-2003 obtained from
547 PCR-GLOBWB (Sutatudjaja et al., 2009) to estimate at 5 arcminute resolution average
548 groundwater level decline rates (m yr^{-1}). Figure S14 in the Supplement shows box plots of
549 streamflow trends and groundwater head trends from the observations and from our
550 framework. The distribution of estimated streamflow decline overlaps with that from the
551 observed trends with a slight underestimation. The observed groundwater head decline rates
552 however are underestimated. This may be caused by the fact that we only have three
553 observations which are from a mostly confined aquifer where small storage coefficients lead
554 to larger decline rates.

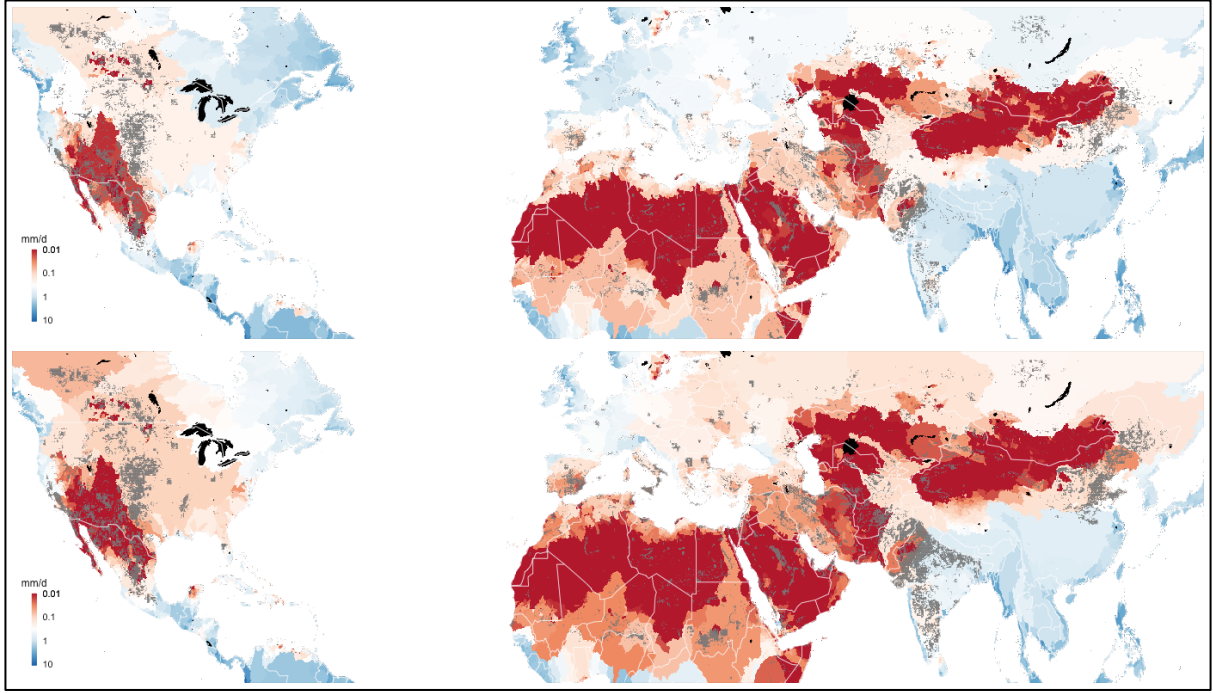
555

556 To further investigate the performance of our method in reproducing groundwater level
557 declines at the sub-basin scale, we compare estimated groundwater level declines between
558 2002-2015 from 1522 groundwater wells in the Republican Basin obtained from McGuire,
559 (2017). Figure S15 shows maps and boxplots of observed groundwater level declines (m) and
560 declines estimated from the analytical framework. Although the overall pattern of
561 groundwater depletion in the Republican Basin is reproduced, there are occasional outliers in
562 the global estimates that are not seen in the observations. This is likely the result from the
563 global withdrawal data that are obtained by downscaling the total US groundwater
564 withdrawal to 5-arcminutes based on 5-arcminute estimates of total groundwater demand
565 (Sutanudjaja et al., 2018). Although these downscaled withdrawal rates are well verified at
566 the county-scale (See Wada et al., 2012), the mismatch at the 5-arcminute scale can be large.
567 Thus, when using global datasets, the analytical framework is limited to the sub-basin scale
568 and too coarse for local-scale estimates. Improvements can be expected when local data on
569 groundwater withdrawal are available at finer resolution.

570

571 ***Critical limits to groundwater withdrawal for major basins***

572 We finish the result section by summarizing critical limits to groundwater withdrawal for the
573 major river basins of the world. In Figure 9a the median value of q_{crit} is plotted for the major
574 basins in the world (sub-watershed level of HydroBasins, Lehner et al., 2008) together with
575 the areas where groundwater withdrawal is on average unstable over the years 2000-2015.
576 This figure provides, at first order, a global map of the maximum limit to physically stable
577 groundwater withdrawal rates. The parts of the world where the critical withdrawal rates are
578 very small largely coincide with the band of countries that experience high values of water
579 stress (Hofsté et al., 2019). This shows that there is little room in these areas to supplement
580 water demand without causing groundwater depletion.



581

582 *Figure 9. Global limits to stable groundwater withdrawal rate; top: limit to physically stable*
 583 *groundwater withdrawal mapped as the median q_{crit} per sub-basin (based on Hydro-basins:*
 584 *Lehner et al., 2008), grey-shaded areas are those for which $q > q_{crit}$; bottom: limit to*
 585 *ecologically stable groundwater withdrawal mapped as the median q_{eco} per sub-basin, grey-*
 586 *shaded areas are those $q > q_{eco}$.*

587

588 The ecological limits to groundwater withdrawal, q_{eco} , can be defined as the withdrawal rate
 589 that is low enough to prevent streamflow from dropping below some environmental flow
 590 limit Q_{env} , i.e. a value that is high enough to safeguard the integrity of the aquatic ecosystems
 591 (Linnansaari et al. 2013; Pastor et al 2014). The value of q_{eco} can be calculated by inverting
 592 Equation (A14) and taking $Q(\infty) < Q_{env}$:

$$593 \quad q_{eco} = \frac{(Q_i + (q_s + r)A) - Q_{env}}{A} \quad (4)$$

594 We note that environmental flows are usually defined during low flow conditions (Pastor et
 595 al 2014; Gleeson and Richter, 2018), so it may be more appropriate to use the value of $Q(\infty)$
 596 as the average over the summer half year instead of yearly averages. If we assume that the
 597 average streamflow regime follows a cosine function with a period of 1 year, then the
 598 average (natural) streamflow Q_s in summer would be equal to:

$$599 \quad Q_s = \left(1 - \frac{2}{\pi}\right) [(Q_i + (q_s + r)A)] \quad (5)$$

600 and q_{eco} becomes:

$$601 \quad q_{eco} = \frac{\left(1 - \frac{2}{\pi}\right) [Q_i + (q_s + r)A] - Q_{env}}{A} \quad (6)$$

602 In Figure 9 (bottom) we have plotted q_{eco} using, as an example, Q_{env} to be 20% of the
603 average natural summer streamflow Q_s . The resulting map can be seen as a first order
604 approximation of the limits to ecologically stable groundwater withdrawal. In most cases,
605 $q_{eco} < q_{crit}$ as is also evident from the larger grey-shaded areas in the bottom figure compared
606 to the top figure. The results suggest that supplementing water demand by groundwater use in
607 the world's water stressed areas is limited under ecological constraints. We stress that the
608 sub-basin scale critical and environmental limits are meant for large-scale environmental
609 assessment, not for local groundwater management.

610

611 **4. Discussion and conclusions**

612

613 We have introduced an analytical framework based on a lumped conceptual model that
614 intends to describe to what extent groundwater withdrawal affects groundwater heads and
615 streamflow under changing regimes of groundwater-surface water interaction. By feeding the
616 framework with the parameters and inputs from a more complex hydrological model (i.e.,
617 PCR-GLOBWB), it can be used as a screening tool for regional-scale groundwater
618 sustainability. i.e., by providing a rich tableau of hydrologically and ecologically relevant
619 outputs at very limited computational costs. Another possible application is in
620 hydroeconomic modelling, where the equations in Table 1 can be used as regionally varying
621 hydrological response functions (Harou et al., 2009; MacEwan et al., 2017) in
622 hydroeconomic optimization – where model evaluations need to be fast - in order to infer
623 socially optimal pumping rates that include environmental externalities.

624

625 The estimated global groundwater and surface water depletion rates were compared with
626 observations and model results at various scales (support and extent), with mixed but overall
627 favourable results up to the sub-basin scale. Results show that the analytical framework
628 provides similar results to that of global hydrological models, but tends to overestimate the
629 groundwater depletion rates from groundwater flow models that account for lateral flow
630 between cells. Also, without calibration, the critical transient times, i.e, the time from
631 commencement of pumping till the detachment of the water table from the stream, as well as
632 the related time to full capture, are order-of-magnitude estimates at best. Finally, when using
633 global datasets, the analytical framework is limited to the sub-basin scale and too coarse for
634 local-scale estimates.

635

636 We stress that output variables that are related to critical environmental limits such as q_{crit} ,
637 q_{eco} , t_{crit} and t_{ef} are difficult to validate directly, particularly at the larger scales at which our
638 framework operates. This would require large-scale pumping experiments or metering of
639 pumping wells in basins while surface water and groundwater are intensively monitored over
640 decades. As such, the critical limits are non-observables calculated with a model that is only
641 partly validated with a limited set of output variables, i.e. groundwater level decline and
642 streamflow depletion. We note however that this limitation is not restricted to our analytical
643 framework, but occurs for any analytical or numerical groundwater model used.

644

645 Clearly, many complicating factors are neglected in our approach, e.g.: underground spatial
646 heterogeneity, including the occurrence of multiple aquifer systems and semi-confined layers
647 that are present in many important alluvial groundwater basins; the variable depth and
648 topology of the surface water system and the intermittent nature of many streams in semi-arid
649 to semi-humid areas; and the locations of the wells with respect to the streams. Of these, the
650 neglect of confining layers may be one of the more crucial limitations of the approach. For
651 instance, a considerable part of the groundwater used for irrigation in the big alluvial basins
652 of the U.S. (e.g. Ogallala and Central Valley of California), where farmers have the financial
653 resources to drill deep wells (Perrone and Jasechko, 2019), is pumped from deeper confined
654 aquifers. This means that the groundwater-surface water interaction is limited to the large
655 rivers and lakes only and that head decline per volume water pumped is larger than in
656 phreatic conditions. It would in principle be possible to include the effect of a confining layer
657 by using a larger value of the groundwater-surface water resistance parameter C , a smaller
658 value of recharge r and a storage coefficient instead of specific yield. Similarly, the impacts
659 of seasonably variable boundary conditions of q , q_s and Q_i could be taken into account by
660 simple convolution, considering that the groundwater level responses $h(t)$ and dh/dt (Table 1)
661 are respectively step and impulse responses of a linear system. Also, the effects of multiple
662 streams with variable stream bottom elevations could be included by extending the piecewise
663 linearization of Equation (2) to more domains (e.g. Bierkens and te Stroet, 2007). However,
664 we argue that such extensions are not in the spirit of the simple analytical framework
665 developed, which intends to provide first order sensitivities at larger scales. If the addition of
666 complexity is needed to provide more accurate assessments for a specific case, it would be
667 more logical to build a tailor-made numerical groundwater flow model.

668

669 We end with the note that a global application of our conceptual analytical framework is not
670 restricted to the use of data from the PCR-GLOBWB repository. The necessary fluxes r , q , Q_i
671 and q_s can also be obtained from other repositories of multi-model re-analyses such as
672 Earth2Observe (Schellekens et al., 2017) and from the combination of remotely sensed
673 estimates of hydrological variables (Lettenmaier et al., 2015; McCabe et al., 2017), e.g.
674 estimating recharge and surface runoff from remotely sensed precipitation, evaporation and
675 soil moisture change, and using high-resolution global datasets on discharge (Barbarossa et
676 al., 2018) and river bed dimensions (Allen and Pavelsky, 2018; Lehner et al., 2018).

677 **Data availability.**

678 The data used in the global assessments provided by PCR-GLOBWB 2 can downloaded
679 from: <https://doi.org/10.4121/uuid:e3ead32c-0c7d-4762-a781-744dbdd9a94b>. The
680 groundwater response times of Cuthbert et al. (2019) can be found on:
681 <https://doi.org/10.6084/m9.figshare.7393304> GRACE data used for validation are obtained
682 from: <https://doi.org/10.5067/TEMSC-OCL05>. The Republican River Basin well data from
683 2002-2015 can be downloaded from <https://pubs.er.usgs.gov/publication/sim3373>.

684

685 **Author contributions.**

686 MB conceived and designed the study. NW and MB performed the calculations. NW and
687 EHS performed the model validation. MB wrote the paper. All authors read, commented on,
688 and revised the manuscript.

689

690 **Competing interests.**

691 The authors declare that they have no conflict of interest.

692

693 **Acknowledgements.**

694 Niko Wanders acknowledges funding from NWO 016.Veni.181.049. The comments and
695 suggestions by the Editor, referee Grant Ferguson and four anonymous referees significantly
696 improved the manuscript.

697 **References**

- 698
- 699 Allen, H. and Pavelsky, M.: Global extent of rivers and streams, *Science* 361, 585-588, 2018.
- 700 Alley, W.M., Reilly, T. E. and Franke, O. L.: Sustainability of groundwater resources, *United*
701 *States Geological Survey Circular*, 1186, 1999.
- 702 Barbarossa, V., Huijbregts, M., Beusen, A. *et al.*: FLO1K, global maps of mean, maximum
703 and minimum annual streamflow at 1 km resolution from 1960 through 2015, *Sci*
704 *Data*, 5, 180052, 2018.
- 705 Bierkens, M.F.P. and Te Stroet, C.B.M.: Modelling non-linear water table dynamics and
706 specific discharge through landscape analysis. *J. Hydrol.*, 332, 412– 426, 2007.
- 707 Bierkens, M.F.P. and Wada, Y.: Non-renewable groundwater use and groundwater depletion:
708 a review. *Environ. Res. Lett.*, 14 063002, 2019.
- 709 Condon, L.E. and Maxwell, R.M.: Simulating the sensitivity of evapotranspiration and
710 streamflow to large-scale groundwater depletion, *Sci. Adv.*, 5, eaav4574, 2019.
- 711 Cuthbert, M.O., Gleeson, T., Moosdorf, N. *et al.* : Global patterns and dynamics of climate–
712 groundwater interactions, *Nature Clim. Change*, 9, 137–141, 2019.
- 713 de Graaf, I.E.M., van Beek, L.P.H., Wada, Y., and Bierkens, M.F.P.: Dynamic attribution of
714 global water demand to surface water and groundwater resources: Effects of abstractions
715 and return flows on river discharges, *Adv. Water Resour.*, 64, 21–33, 2014.
- 716 de Graaf, I.E.M., Gleeson, T., van Beek, L.P.H., Sutanudjaja, E.H. and Bierkens, M.F.P.:
717 Environmental flow limits to global groundwater pumping, *Nature*, 574, 90-108, 2019.
- 718 Döll, P., Müller Schmied, H., Schuh, C., Portmann, F.T. and Eicker, A.: Global-scale
719 assessment of groundwater depletion and related groundwater abstractions: Combining
720 hydrological modeling with information from well observations and GRACE satellites,
721 *Water Resour. Res.*, 50, 5698–5720, 2014.
- 722 Elmore, A.J., Manning, S.J., Mustar, J.F. and Craine J.M.: Decline in alkali meadow
723 vegetation cover in California: the effect of groundwater extraction and drought, *J. Appl.*
724 *Ecol.*, 43, 770–9, 2006.
- 725 Gleeson, T., Moosdorf, N., Hartmann, J., and van Beek, L.P.H.: A glimpse beneath earth's
726 surface: GLobal HYdrogeology MaPS (GLHYMPS) of permeability and porosity,
727 *Geophys. Res. Lett.*, 41, 3891–3898, 2014.
- 728 Gleeson, T. and Richter, B.: How much groundwater can we pump and protect environmental
729 flows through time? Presumptive standards for conjunctive management of aquifers and
730 rivers, *River Res. Appl.*, 34, 83–92, 2018.
- 731 Godfray, H.C.J., Beddington, J.R, Crute, I.R., Haddad, L., Lawrence, D., Muir, J.F. et al.:
732 Food security: The challenge of feeding 9 billion people. *Science*, 327, 812–818. 2010.
- 733 Harou, J.J., Pulido-Velazquez, M., Rosenberg, D.E., Medellín-Azuara, J., Lund, J. R. and
734 Howitt, R.E.: Hydro-economic models: concepts, design, applications, and future
735 prospects, *J. Hydrol.*, 375 627–43, 2009.
- 736 Hofste, R.W.,Kuzma, S., Walker, S., Sutanudjaja, E.H., Bierkens, M.F.P., Kujiper, M.J.M.,
737 Sanchez, M.F., van Beek, R., Wada, Y., Rodríguez, S.G.: *Aqueduct 3.0: Updated*
738 *Decision-Relevant Global Water Risk Indicators*; Technical Note World Resources
739 Institute, Washington, DC, USA; <https://www.wri.org/publication/aqueduct-30>, 2019.
- 740

741 Huang, S.-H., Yang, T. and Yeh, H.-D. (2018). Review of analytical models to stream
742 depletion induced by pumping: Guide to model selection. *J. Hydrol*, 561, 277-285.

743 Hunt, B.: Unsteady stream depletion when pumping from semiconfined aquifers, *J. Hydrol.*
744 *Eng.-ASCE*, 8, 12–19, 2018.

745 Jasechko, S., Seybold, H., Perrone, D., Fan, Y. and Kirchner, J.: Widespread potential loss of
746 streamflow into underlying aquifers across the USA, *Nature*, 591, 391–395, 2021.

747 Konikow, L.F. and Leake, S.A.: Depletion and capture: Revisiting “the source of water
748 derived from wells”, *Groundwater*, 52, 100–111, 2014.

749 Kraijenhoff van de Leur, D. A.: A study of non-steady ground-water flow with special
750 reference to the reservoir-coefficient, *De Ingenieur*, 19, 87–94, 1958.

751 Lehner, B., Verdin, K. and Jarvis, A.: New global hydrography derived from spaceborne
752 elevation data, *Eos*, 89, 93–94, 2008.

753 Lehner, B., Ouellet Dallaire, C., Ariwi, J., Grill, G., Anand, M., Beames, P., Burchard-
754 Levine, V., Maxwell, S., Moidu, H., Tan, F. and Thieme, M.: Global hydro-environmental
755 sub-basin and river reach characteristics at high spatial resolution, *Sci. Data*, 6, 283, 2019.

756 Lettenmaier, D. P., Alsdorf, D., Dozier, J., Huffman, G.J., Pan, M. and Wood, E.F.: Inroads
757 of remote sensing into hydrologic science during the WRR era, *Water Resour. Res.* 51,
758 7309–7342, 2015.

759 Linnansaari T, Monk, W.A., Baird, D.J. and Curry R.A.: *Review of Approaches and Methods*
760 *to Assess Environmental Flows Across Canada and Internationally*. Canadian Science
761 Advisory Secretariat, Research Document 2012/039, New Brunswick, Department of
762 Fisheries and Oceans Canada, 2013.

763 MacDonald, A., Bonsor, H., Ahmed, K. *et al.*: Groundwater quality and depletion in the
764 Indo-Gangetic Basin mapped from *in situ* observations, *Nature Geosci.*, 9, 762–766, 2016.

765 MacEwan, D., Cayar, M., Taghavi, A., Mitchell, D., Hatchett, S. and Howitt, R.:
766 Hydroeconomic modeling of stable groundwater management, *Water Resour. Res.*, 53
767 2384–403, 2017.

768 McCabe, M. F., Rodell, M., Alsdorf, D. E., Miralles, D. G., Uijlenhoet, R., Wagner, W.,
769 Lucieer, A., Houborg, R., Verhoest, N. E. C., Franz, T. E., Shi, J., Gao, H., and Wood,
770 E.F.: The future of Earth observation in hydrology, *Hydrol. Earth Syst. Sci.*, 21, 3879–
771 3914, 2017.

772 McGuire, V.L.: *Water-level changes in the High Plains aquifer, Republican River Basin in*
773 *Colorado, Kansas, and Nebraska, 2002 to 2015 (ver. 1.2, March 2017)*, U.S. Geological
774 Survey Scientific Investigations Map 3373, 10 p., 1 sheet with appendix,
775 <https://doi.org/10.3133/sim3373>, 2017.

776 Mukherjee, A., Bhanja, S.N. and Wada, Y.: Groundwater depletion causing reduction of
777 baseflow triggering Ganges river summer drying, *Sci. Rep.*, 8, 12049, 2018.

778 Pastor, A.V., Ludwig, F., Biemans, H., Hoff, H. and Kabat, P.: Accounting for environmental
779 flow requirements in global water assessments, *Hydrol. Earth Syst. Sci.*, 18, 5041–5059,
780 2014.

781 Perrone, D. and Jasechko, S.: Deeper well drilling an unstable stopgap to groundwater
782 depletion, *Nat. Sustain.*, 2, 773–782, 2019.

783 Richey, A. S., Thomas, B. F., Lo, M.-H., Reager, J.T., Famiglietti, J.S., Voss, K., Swenson,
784 S. and Rodell, M.: Quantifying renewable groundwater stress with GRACE, *Water*
785 *Resour. Res.*, 51, 5217–5238, 2015.

786 Runhaar ,H., Witte, J.P.M. and Verburg, P.: Groundwater level, moisture supply, and
787 vegetation in the Netherlands, *Wetlands*, 17, 528–38, 1997.

788 Scanlon, B.R., Faunt, C.C., Longuevergne, L., Reedy, R.C., Alley, W.M., McGuire, V.L. and
789 McMahon, P.B.: Groundwater depletion and sustainability of irrigation in the U.S. High
790 Plains and Central Valley, *Proc. Nat. Acad. Sci. U.S.A.*, 109, 9320–9325, 2012.

791 Schellekens, J., Dutra, E., Martínez-de la Torre, A., Balsamo, G., van Dijk, A., Sperna
792 Weiland, F., Minvielle, M., Calvet, J.-C., Decharme, B., Eisner, S., Fink, G., Flörke, M.,
793 Peßenteiner, S., van Beek, R., Polcher, J., Beck, H., Orth, R., Calton, B., Burke, S.,
794 Dorigo, W., and Weedon, G. P.: A global water resources ensemble of hydrological
795 models: the earth2Observe Tier-1 dataset. *Earth Syst. Sci. Data*, 9, 389–413, 2017.

796 Shafroth P.B., Stromberg J.C. and Patten D.T.: Woody riparian vegetation response to
797 different alluvial water table regimes Western North, *Am. Nat.*, 60, 66–76, 2000.

798 Siebert, S., Kummu, M., Porkka, M., Döll, P., Ramankutty, N. and Scanlon, B.R.: A global
799 data set of the extent of irrigated land from 1900 to 2005, *Hydrol. Earth Syst. Sci.*, 19,
800 1521–1545, 2015.

801 Sutanudjaja, E. H., van Beek, R., Wanders, N., Wada, Y., Bosmans, J. H. C., Drost, N., van
802 der Ent, R. J., de Graaf, I. E. M., Hoch, J. M., de Jong, K., Karssenber, D., López López,
803 P., Peßenteiner, S., Schmitz, O., Straatsma, M. W., Vannamettee, E., Wisser, D., and
804 Bierkens, M.F.P.: PCR-GLOBWB 2: a 5 arcmin global hydrological and water resources
805 model, *Geosci. Model Dev.*, 11, 2429–2453, 2018.

806 Theis, C.V.: The source of water derived from wells, *Civ. Eng.*, 10, 277–280, 1940.

807 Bredehoeft, J.D.: The water budget myth revisited: why hydrogeologists model,
808 *Groundwater*, 40, 340-345, 2002.

809 Wada, Y., van Beek, L.P.H. van Kempen, C.M., Reckman, J.W.T., Vasak, S., and Bierkens,
810 M.F.P.: Global depletion of groundwater resources, *Geoph. Res. Lett.*, 37, L20402, 2010.

811 Wada, Y., van Beek, L.P.H. and Bierkens, M.F.P: Nonstable groundwater sustaining
812 irrigation: A global assessment, *Water Resour. Res.*, 48, W00L06, 2012.

813 Wada Y., van Beek, L.P.H., Wanders and Bierkens M.F.P. (2013). Human water
814 consumption intensifies hydrological drought worldwide. *Environ. Res. Lett.* 8, 034036.

815 Wada Y.: Modeling Groundwater Depletion at Regional and Global Scales: Present State and
816 Future Prospects, *Surv. Geophys.*, 37, 419–451, 2016.

817 Watkins, M.M., Wiese, D.N., Yuan, D.-N., Boening, C., and Landerer, F.W.: Improved
818 methods for observing Earth's time variable mass distribution with GRACE using
819 spherical cap mascons, *J. Geophys. Res.-Solid*, 120, 2648–2671, 2015.

820 Wen, F. and Chen, X.: Evaluation of the impact of groundwater irrigation on streamflow in
821 Nebraska, *J. Hydrol.*, 327, 603-617, 2006.

822 Wiese, D.N.: GRACE monthly global water mass grids NETCDF RELEASE 5.0,
823 Version 5.0, PO.DAAC, CA, USA, Dataset, available at: [https://doi.org/10.5067/TEMSC-](https://doi.org/10.5067/TEMSC-OCL05)
824 [OCL05](https://doi.org/10.5067/TEMSC-OCL05) (last access: 15 September 2017), 2015.

825 Wiese, D.N., Landerer, F.W., and Watkins, M.M.: Quantifying and reducing leakage errors in
826 the JPL RL05M GRACE mascon solution, *Water Resour. Res.*, 52, 7490–7502, 2016.

- 827 Winter, T.C., Harvey, J.W., Franke, O.L. and Alley, W.A.: *Ground water and surface water:*
828 *A single resource*, U.S. Geol. Surv. Circ., 1139, 1998.
- 829 Yin, L., Zhou, Y., Xu, D., Zhang, J., Wang, X., Ma, H. and Dong, J.: Response of
830 phreatophytes to short-term groundwater withdrawal in a semiarid region: Field
831 experiments and numerical simulations, *Ecohydrol.*, 11, e1948, 2018.
- 832 Zipper, S.C., Dallemagne, T., Gleeson, T., Boerman, T.C., and Hartmann, A.: Groundwater
833 pumping impacts on real stream networks: Testing the performance of simple
834 management tools, *Water Resour. Res.*, 54, 5471-5486, 2018.

835 **Appendix A: Conceptual model for regional-scale groundwater pumping**
 836 **with groundwater-surface water interaction**

837
838

839 **A1. Basic equations**

840 We repeat the three basic equations that make up the lumped conceptual model of regional-
 841 scale groundwater pumping with groundwater-surface water interaction:

842 The groundwater head as described with the total aquifer mass balance:

843
$$n \frac{dh}{dt} = r + F_{gw \leftrightarrow sw}(h) - q \quad (A1)$$

844 The groundwater - surface water flux:

845
$$F_{gw \leftrightarrow sw}(h) = \begin{cases} -\frac{h-h_s}{c} & h \geq d \\ \frac{h_s-d}{c} & h < d \end{cases} \quad (A2)$$

846 The surface water balance:

847
$$Q = Wv(h_s - d) = Q_i + q_s A - F_{gw \leftrightarrow sw}(h)A \quad (A3)$$

848

849 **A2. The case $h(t) \geq d$ and $q < q_{crit}$**

850 We will start by analyzing the case that $h \geq d$, i.e. the groundwater level is attached to the
 851 surface water body. We further assume that $q < q_{crit}$, i.e. the groundwater withdrawal is such
 852 that the groundwater level never falls below the surface water bottom level d . In this case, the
 853 surface water flux Q (m³/d) is related to the groundwater and surface water level as follows

854 (See Figure A1):

855
$$Q = Wv(h_s - d) = Q_i + q_s A + \frac{h-h_s}{c} A \quad (A3)$$

856 with

857 A : The area over (sub-)aquifer considered (m²)

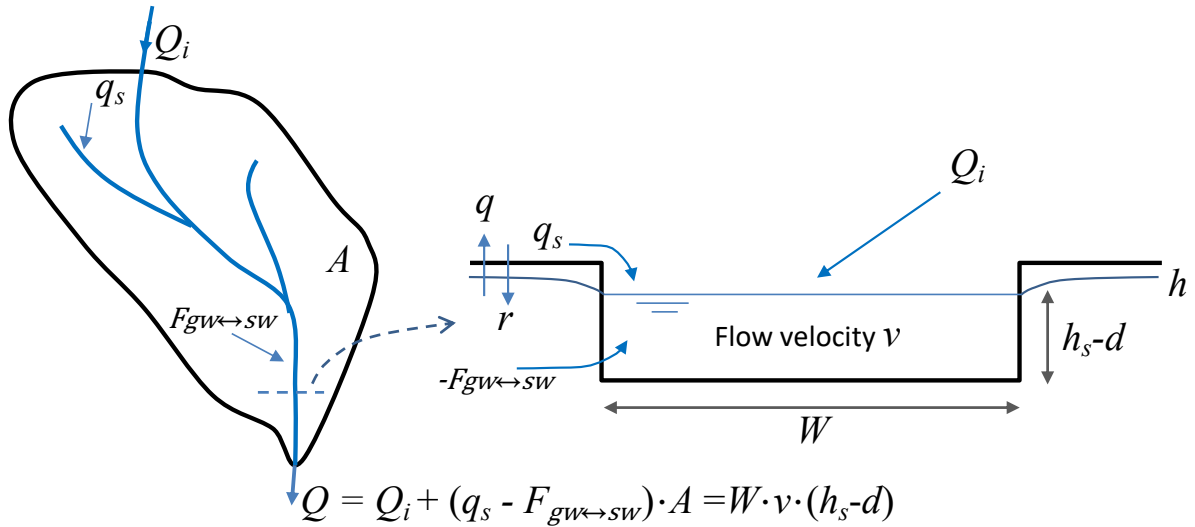
858 q_s : surface runoff (m yr⁻¹)

859 Q_i : influx of surface water from upstream (m³ yr⁻¹)

860 W : Stream width (m)

861 d : Bottom elevation stream (m)

862 v : Stream flow velocity (m yr⁻¹)



863

864 *Figure A1. Contributing fluxes to streamflow.*

865

866 Collecting h_s on one side and the other terms on right side results in the following relation

867 between surface water height and groundwater head:

$$868 \quad h_s(t) = \alpha + \beta h(t) \quad (A4)$$

869 with

$$870 \quad \alpha = \frac{Q_i c + q_s A c + W v d c}{W v c + A} \quad (A5)$$

$$871 \quad \beta = \frac{A}{W v c + A} \quad (A6)$$

872 From (A1) and (A2) the differential equation for groundwater level gives:

$$873 \quad n \frac{dh}{dt} = r - \frac{h - h_s}{c} - q \quad (A7)$$

874 And after substituting (A4)

$$875 \quad \Rightarrow n \frac{dh}{dt} = \left(r + \frac{\alpha}{c} - q \right) - \left(\frac{1 - \beta}{c} \right) h \quad (A8)$$

876 From (A8) follows the steady-state groundwater level under natural conditions ($q = 0$ and

877 $dh/dt = 0$):

$$878 \quad \bar{h}_{nat} = \frac{r c + \alpha}{1 - \beta} \quad (A9)$$

879 Solving differential equation (A8) for initial condition (A9) then yields:

$$880 \quad h(t) = \frac{r c + \alpha}{1 - \beta} - \left(\frac{q c}{1 - \beta} \right) \left[1 - e^{-\left(\frac{1 - \beta}{n c} \right) t} \right] \quad (A10)$$

881 Which also gives the equilibrium groundwater level for $t \rightarrow \infty$:

$$882 \quad h(\infty) = \frac{r c + \alpha - q c}{1 - \beta} \quad (A11)$$

883 The surface water level with time is given by (A4) and the final equilibrium surface water

884 follows from (A4) and (A11) as:

885
$$h_s(\infty) = \alpha + \frac{\beta(rc + \alpha - qc)}{1 - \beta} \quad (\text{A12})$$

886 The surface water discharge as a function of time follows from combining (A3) and (A4):

887
$$Q(t) = Q_i + q_s A - \frac{A\alpha}{c} + \frac{A(1-\beta)}{c} h(t) \quad (\text{A13})$$

888 with $h(t)$ given by (A10). The equilibrium discharge is obtained by substituting (A11) for
889 $h(\infty)$ in (A13):

890
$$Q(\infty) = Q_i + (q_s + r - q)A \quad (\text{A14})$$

891 Which also follows logically from the water balance.

892

893 **A3. The critical withdrawal rate q_{crit}**

894 The critical withdrawal rate determines whether at larger times the water table drops below
895 the bottom of the surface and moves to the physically unstable regime. We seek q such that
896 $h(\infty) = d$:

897
$$\frac{rc + \alpha - qc}{1 - \beta} = d \quad (\text{A15})$$

898 From which follows:

899
$$q = \frac{rc + \alpha - d(1 - \beta)}{c} \quad (\text{A16})$$

900 Substituting α and β yields after some manipulation:

901
$$q_{\text{crit}} = r + \frac{Q_i + q_s A}{Wvc + A} \quad (\text{A17})$$

902

903 **A4. Critical transition time t_{crit} in case $q > q_{\text{crit}}$**

904 In case $q > q_{\text{crit}}$ at some time after pumping (t_{crit}) the groundwater level will fall below the
905 bottom elevation d of the surface water. Before that time, it follows the water table decline
906 according to (A10). So, we can find t_{crit} by solving it from:

907
$$h(t_{\text{crit}}) = \frac{rc + \alpha}{1 - \beta} - \left(\frac{qc}{1 - \beta}\right) \left[1 - e^{-\left(\frac{1 - \beta}{nc}\right)t_{\text{crit}}}\right] = d \quad (\text{A18})$$

908 Solving an equation of the form $a - b[1 - e^{-cx}] = d$ gives as solution: $x = \frac{1}{c} \ln \left(\frac{b}{d - a + b}\right)$

909 from which follows from (A18):

910
$$t_{\text{crit}} = \frac{nc}{1 - \beta} \ln \left(\frac{qc}{qc - (rc + \alpha) + d(1 - \beta)}\right) \quad (\text{A19})$$

911

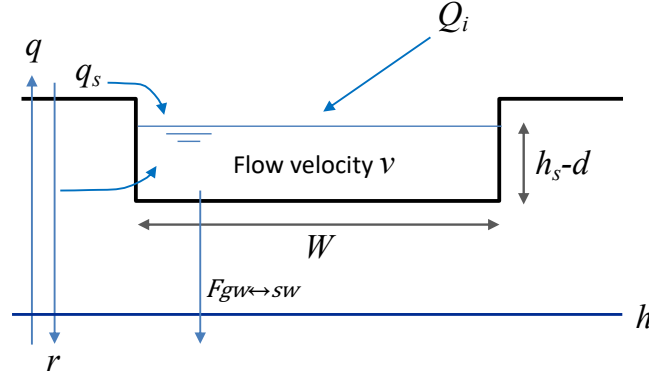
912 **A5. The case $q > q_{\text{crit}}$ and $t > t_{\text{crit}}$ ($h(t) < d$)**

913 In case the water table is below the bottom elevation of the stream, the water balance of the
914 stream reads (see Fig. A2):

915
$$Q = Wv(h_s - d) = Q_i + q_s A - \frac{h_s - d}{c} A \quad (A20)$$

916 From which we can derive an equation for the minimum and constant elevation of the surface
 917 water level (valid for $t > t_{crit}$):

918
$$h_s = d + \frac{(Q_i + q_s A)c}{WvC + A} \quad (A21)$$



919
 920 *Figure A2. Water balance of a stream in case $q > q_{crit}$ and $t > t_{crit}$ ($h(t) < d$)*

921
 922 The differential equation describing the change in groundwater with time now becomes:

923
$$n \frac{dh}{dt} = r - q + \frac{h_s - d}{c} \quad (A22)$$

924 Substituting $h_s - d$ from (A21) then yields an equation for the groundwater decline rate:

925
$$\frac{dh}{dt} = \frac{r - q}{n} + \frac{(Q_i + q_s A)}{n(WvC + A)} \quad (A23)$$

926 which is always negative since $q > q_{crit}$. With initial condition $h(t_{crit}) = d$ one obtains from
 927 (A23) and equation for $h(t)$, $t > t_{crit}$:

928
$$h(t) = d + \left[\frac{r - q}{n} + \frac{(Q_i + q_s A)}{n(WvC + A)} \right] (t - t_{crit}) \quad (A24)$$

929
 930 **A5. Sources of pumped groundwater: $q < q_{crit}$ or $t < t_{crit}$ ($h(t) \geq d$)**

931 When neglecting direct evaporation from groundwater, the sources of pumped groundwater
 932 in case $q < q_{crit}$ either come out of storage or from recharge that does not contribute to
 933 streamflow. The latter is called “capture”. From the water balance (A1) we thus find:

934
$$q = r + F_{gw \leftrightarrow sw}(h(t)) - n \frac{dh}{dt} \quad (A25)$$

935 The first two terms constitute the water pumped from capture (with $F_{gw \leftrightarrow sw}$ negative in case
 936 $h > h_s$ and positive when $h < h_s$) and the second term the water out of storage. Furthermore,
 937 from differentiation of (A10) we have:

938
$$n \frac{dh}{dt} = -q e^{-\left(\frac{1-\beta}{nC}\right)t} \quad (\text{A26})$$

939 Combining (A26) and (A25) then gives (since capture + out of storage add up to q):

940

941
$$q = \underbrace{q \left(1 - e^{-\left(\frac{1-\beta}{nC}\right)t}\right)}_{r + F_{gw \leftrightarrow sw}} + \underbrace{q e^{-\left(\frac{1-\beta}{nC}\right)t}}_{-n \frac{dh}{dt}} \quad (\text{A27})$$

942

943

944 This shows that the fraction groundwater taken out of storage reduces over time until head
945 decline stops and all water comes out of capture.

946

947 **A6. Sources of pumped groundwater: $q > q_{crit}$ and $t > t_{crit}$ ($h(t) < d$)**

948 In case $q > q_{crit}$ and $t < t_{crit}$ the sources of pumped groundwater follow (A27). After the
949 groundwater table falls below the bottom elevation of the stream and $t > t_{crit}$ the sources of
950 water follow from (A23):

951
$$n \frac{dh}{dt} = r - q + \frac{(Q_i + q_s A)}{(WvC + A)} \quad (\text{A28})$$

952 And therefore:

953
$$q = r + \frac{(Q_i + q_s A)}{(WvC + A)} - n \frac{dh}{dt} \quad (\text{A29})$$

954 Since the third term is the storage change and capture plus storage change add up to q we
955 have:

956
$$q = \underbrace{r + \frac{(Q_i + q_s A)}{(WvC + A)}}_{r + F_{gw \leftrightarrow sw}} + \underbrace{q - \left(r + \frac{(Q_i + q_s A)}{(WvC + A)}\right)}_{-n \frac{dh}{dt}} \quad (\text{A30})$$

957

958

959 which shows that at after $t > t_{crit}$ the ratio of pumping from capture (i.e. recharge and surface
960 water leakage) and storage change becomes constant.

961

962

963 **Appendix B: Relationship between groundwater response time J and**
964 **drainage resistance C**

965
966 In PCR-GLOBWB 2 (Sutanudjaja et al., 2018) and in similar global hydrological models, the
967 relationship between groundwater discharge Q_g ($\text{m}^3 \text{m}^{-2} \text{d}^{-1}$) and the volume V_g (m^3/m^2)
968 stored in the groundwater store is given by a simple linear relationship:

969
$$Q_g = \frac{V_g}{J} \tag{B1}$$

970

971 With J the characteristic response time of the groundwater system (e-folding time of the
972 recession) (yr). In some of the global models J is obtained by calibration to low flows or
973 recession curves. In PCR-GLOBWB it is calculated from transient drainage theory of
974 Kraijenhoff-van de Leur (1958) as:

975
$$J = \frac{nL^2}{\pi^2 T} \tag{B2}$$

976

977 with n the drainable porosity or specific yield, L the average distance between water courses
978 (derived from the drainage density per cell) and T the aquifer transmissivity obtained from
979 global hydrogeological datasets (e.g. Gleeson et al., 2014). A similar approach was used by
980 Cuthbert et al. (2019) to derive groundwater response times.

981

982 The drainable volume of groundwater stored in the groundwater reservoir ($\text{m}^3 \text{m}^{-2}$) of a grid
983 cell of a global hydrological model can also be expressed as: $V_g = n(h - h_s)$, with h_s the
984 surface water level and h the groundwater level in the cell. Substituting this into (B1) we
985 obtain the equivalent groundwater drainage equation for a grid cell:

986
$$Q_g = \frac{n(h-h_s)}{J} \tag{B3}$$

987

988 Comparing (B3) with (A2) shows that to obtain the same groundwater-surface water
989 exchange in the global hydrological model and the conceptual analytical model we must
990 have:

991
$$C = \frac{J}{n} \tag{B4}$$

992

993 Note that these relationships assume that the streams remain connected with the surface
994 water, which is not entirely consistent with Equation A2.